NAVAL POSTGRADUATE SCHOOL

Monterey, California

THESIS

NATURAL CONVECTION
ABOVE
A HORIZONTAL HEAT SOURCE

by

Adrian J. Jansen

March, 1993

Thesis Advisor: Yogendra Joshi

Approved for public release; distribution is unlimited

Unclassified

SECURITY CLASSIFICATION OF THIS PAGE

REPORT DOCUMENTATION PAGE

1a. REPORT SECURITY CLASSIFICATION Unclassified	1b. RESTRICTIVE MARKINGS
2a. SECURITY CLASSIFICATION AUTHORITY	3. DISTRIBUTION/AVAILABILITY OF REPORT Approved for public release; distribution is unlimited.
2b. DECLASSIFICATION/DOWNGRADING SCHEDULE	
4. PERFORMING ORGANIZATION REPORT NUMBER(S)	5. MONITORING ORGANIZATION REPORT NUMBER(S)
6a. NAME OF PERFORMING ORGANIZATION Naval Postgraduate School 6b. OFFICE SYMBOL (*If applicable*) ME	7a. NAME OF MONITORING ORGANIZATION Naval Postgraduate School
6c. ADDRESS (*City, State, and ZIP Code*) Monterey, CA 93943-5000	7b. ADDRESS (*City, State, and ZIP Code*) Monterey, CA 93943-5000
8a. NAME OF FUNDING/SPONSORING ORGANIZATION 8b. OFFICE SYMBOL (*If applicable*)	9. PROCUREMENT INSTRUMENT IDENTIFICATION NUMBER
8c. ADDRESS (*City, State, and ZIP Code*)	10. SOURCE OF FUNDING NUMBERS Program Element No. / Project No / Task No / Work Unit Accession Number

11. TITLE (*Include Security Classification*)
NATURAL CONVECTION ABOVE A HORIZONTAL HEAT SOURCE

12. PERSONAL AUTHOR(S) Adrian J. Jansen

13a. TYPE OF REPORT	13b. TIME COVERED	14. DATE OF REPORT (*year, month, day*)	15. PAGE COUNT
Master's Thesis	From To	March 1993	74

16. SUPPLEMENTARY NOTATION
The views expressed in this thesis are those of the author and do not reflect the official policy or position of the Department of Defense or the U.S. Government.

17. COSATI CODES			18. SUBJECT TERMS (*continue on reverse if necessary and identify by block number*)
FIELD	GROUP	SUBGROUP	Natural convection, square heat source, buoyant plume

19. ABSTRACT (*continue on reverse if necessary and identify by block number*)

An investigation of natural convection heat transfer from a flush mounted heater on a larger horizontal substrate in water has been conducted. The focus of the present investigation was on the buoyant flow above the heat source. Temperature measurements in the buoyant plume were made at various locations and heights, for a number of input powers using a traversing thermocouple probe. Simple signal processing was performed on the temperature measurements to attempt to investigate the reported meandering motions in the plume and the transition from laminar to turbulent buoyant flow. These measurments are interpreted based on flow visualizations.

20. DISTRIBUTION/AVAILABILITY OF ABSTRACT	21. ABSTRACT SECURITY CLASSIFICATION	
☒ UNCLASSIFIED/UNLIMITED ☐ SAME AS REPORT ☐ DTIC USERS	Unclassified	
22a. NAME OF RESPONSIBLE INDIVIDUAL Yogendra Joshi	22b. TELEPHONE (*Include Area code*) (408) 656-3400	22c. OFFICE SYMBOL ME/Jo

DD FORM 1473, 84 MAR 83 APR edition may be used until exhausted
All other editions are obsolete

SECURITY CLASSIFICATION OF THIS PAGE
Unclassified

Approved for public release; distribution is unlimited.

Natural Convection
Above
a Horizontal Heat Source

by

Adrian J. Jansen
Lieutenant, United States Navy
B.A., University of California, Los Angeles, 1984

Submitted in partial fulfillment
of the requirements for the degree of

MASTER OF SCIENCE IN MECHANICAL ENGINEERING

from the

NAVAL POSTGRADUATE SCHOOL
March, 1993

Author: Adrian J. Jansen
Adrian J. Jansen

Approved by: Yogendra Joshi
Yogendra Joshi, Thesis Advisor

Matthew Kelleher
Matthew D. Kelleher, Chairman
Department of Mechanical Engineering

ABSTRACT

An investigation of natural convection heat transfer from a flush mounted heater on a larger horizontal substrate in water has been conducted. The focus of the present investigation was on the buoyant flow above the heat source. Temperature measurements in the buoyant plume were made at various locations and heights, for a number of input powers using a traversing thermocouple probe. Simple signal processing was performed on the temperature measurements to attempt to investigate the reported meandering motions in the plume and the transition from laminar to turbulent buoyant flow. These measurements are interpreted based on flow visualizations.

TABLE OF CONTENTS

I. INTRODUCTION 1

A. NATURAL CONVECTION ABOVE A HORIZONTAL HEATED FLAT PLATE 1

B. BUOYANT PLUME ABOVE HEATED HORIZONTAL SURFACE . 3

C. PRESENT STUDY 4

II. EXPERIMENTAL APPARATUS AND PROCEDURES 6

A. EXPERIMENTAL APPARATUS 6

1. Test Surface 8

2. Power Supply System 11

3. Thermocouple Probe Traversing System 12

4. Data Acquisition/Reduction System 13

5. Secondary Systems 14

B. EXPERIMENTAL PROCEDURE 15

1. Test Surface Temperature Evaluation 16

2. Buoyant Plume Temperature Measurements . . . 16

3. Flow Visualization 17

III. ANALYSIS OF FLOW VISUALIZATION 18

A. LOW POWER OBSERVATIONS 19

B. MEDIUM POWER OBSERVATIONS 19

C. HIGH POWER OBSERVATIONS 23

IV. ANALYSIS OF PLUME TEMPERATURE DATA 24
A. LOW POWER OBSERVATIONS 25
B. MEDIUM POWER OBSERVATIONS 28
C. HIGH POWER OBSERVATIONS 31
D. COMBINED ANALYSIS 43
1. Laminar Buoyant Flow Above The Surface . . . 44
2. Plume Meandering 45
3. Plume Transition Region 45
4. Turbulent Buoyant Flow 46

V. TEST SURFACE TEMPERATURE ANALYSIS 47
A. CONSTANT POWER 47
B. PERIODIC INPUT POWER 51

VI. CONCLUSIONS 52

VII. RECOMMENDATIONS 53

APPENDIX A 54
1. Characteristic Dimensions. 54
2. Convective Heat Flux. 54
3. Fluid Properties [Ref. 17]. 54
4. Non-dimensional Frequency. 55
5. Modified Grashof Number. 55
6. Nusselt Number. 55
7. Rayleigh Numbers. 55

APPENDIX B 57

1. Frequency Uncertainty. 58

2. Modified Grashof Number Uncertainty. 59

3. Nusselt Number Uncertainty. 59

4. Rayleigh Number Uncertainty. 60

LIST OF REFERENCES 61

INITIAL DISTRIBUTION LIST 63

LIST OF FIGURES

Figure 1. Top View of the Experimental Apparatus. . . 7

Figure 2. Thermocouple Locations under Test Heater. . 8

Figure 3. Bottom View of Test Heater. 10

Figure 4. Power Supply System. 11

Figure 5. Thermocouple Probe. 13

Figure 6. Flow Visualization System. 14

Figure 7. Buoyant Plume at Low Power (3.2 W) (top) 60 second exposure time (bottom) 120 second exposure time. 20

Figure 8. Buoyant Plume Medium Power (19.8 W - 60 second exposure time) (top) steady (bottom) pulsatile. . . 22

Figure 9. Buoyant Plume at High Power (48.9 W - 60 second exposure time). 23

Figure 10. Example of Time Series and FFT/PSD Plots. . 25

Figure 11. Time Series along Plume Centerline at 0.78 W. 26

Figure 12. FFT/PSD along Plume Centerline at 0.78 W. . 26

Figure 13. Time Series along Plume Centerline at 3.2 W. 29

Figure 14. FFT/PSD along Plume Centerline at 3.2 W. . 30

Figure 15. Time Series along Plume Centerline at 12.2 W. 32

Figure 16. FFT/PSD along Plume Centerline at 12.2 W. . 32

Figure 17. Time Series along Plume Centerline at 19.8 W. 32
Figure 18. FFT/PSD along Plume Centerline at 19.8 W . 32
Figure 19. Time Series along Plume Centerline at 27.8 W. 37
Figure 20. FFT/PSD along Plume Centerline at 27.8 W. . 38
Figure 21. Time Series along Plume Centerline at 37.7 W. 39
Figure 22. FFT/PSD along Plume Centerline at 37.7 W. . 40
Figure 23. Time Series along Plume Centerline at 48.9 W. 41
Figure 24. FFT/PSD along Plume Centerline at 48.9 W. . 42
Figure 25. Non-dimensional Frequency versus Grashof Number. 44
Figure 26. Heater Surface Temperatures at Constant Power. 47
Figure 27. Average Nusselt Number versus Flux Based Rayleigh Number. 49
Figure 28. Average Nusselt Number versus Temperature Based Rayleigh Number. 50

ACKNOWLEDGMENT

If riches can be considered a measure of success, then the wealth of knowledge displayed by the faculty of the Mechanical Engineering Department puts NPS at the top of the list. And one of the greatest assets of this department is Professor Yogendra Joshi, whose dedication to learning makes him a true academician. Jim Scholfield, Tom Christian, and Mardo Blanco whose contributions to the students of this department would sorely be missed, are the assets that complete our portfolio. Thank you all.

I. INTRODUCTION

A. NATURAL CONVECTION ABOVE A HORIZONTAL HEATED FLAT PLATE

Natural convection heat transfer from flat surfaces continues to be an area of study that requires further research. Many scientific and engineering applications, such as meteorological thermal rises or plumes emanating from the Earth's surface, are driven by natural convection heat transfer. Investigations of this mode of heat transfer from flat surfaces have been conducted for a variety of planforms and orientations, and using a variety of techniques.

Husar and Sparrow [Ref. 1] researched the nature of free convection flow fields, emphasizing the influence of the heated area on the shape of the fields near the surface. They showed that the flow is normal from of the edge of the surface towards the center. Depending on the planform, bisectors are created by the colliding flow paths as the boundary layer develops into an ascending plume. Ackroyd [Ref. 2] developed a numerical analysis based on, and in good agreement with, the experimental results obtained by Husar and Sparrow.

Goldstein et. al. [Ref. 3] investigated the natural convection mass transfer adjacent to a horizontal downward-facing plate. Using a naphthalene sublimation technique, a common correlation for horizontal plates with specific

characteristic lengths in the Sherwood and Rayleigh numbers was obtained. The results were compared to a number of other studies and some differences were noted due to deviations in geometry and experimental technique. Lloyd and Moran [Ref. 4] used an electrochemical technique to measure mass transfer. They developed correlations for turbulent and laminar mass transfer, the latter agreeing with Goldstein et. al.

In the field of meteorology, natural convection in a large body of fluid leading to freely rising plumes is of great concern. This led Pera and Gebhart [Ref. 5] to conduct analysis and experiment for horizontal and slightly inclined surfaces. Using interferograms, a comparison was made between analytical and experimental results which were found to be in fair agreement depending on Prantl and Grashof numbers. Pera and Gebhart [Ref. 6] then repeated their investigation to include small disturbances. Again, using interferograms, their goal was to compare an analysis of the stability of flow subjected to small disturbances, to experimental results in order to provide greater insight into instability and flow transition.

Al-Arabi and El-Reidy [Ref. 7] studied natural convection over heated isothermal plates. Investigating a number of planforms, they developed new local and average heat transfer correlations for both laminar and turbulent boundary layers. Compared to equations developed by Fishenden and Saunders, the

results obtained for the laminar case were 30% higher and for the turbulent case 11% higher.

Natural convection from a horizontal flat heater, flush mounted in an unheated substrate, was studied by Hickey [Ref. 8]. Hickey investigated the effects of both steady and pulsatile input powers on the surface. A correlation for the resulting natural convection heat transfer was developed. From the data obtained for pulsatile input powers it was noted that the effect of pulsations resulted in minimal heat transfer enhancement as compared to similar steady power inputs.

B. BUOYANT PLUME ABOVE HEATED HORIZONTAL SURFACE

Free boundary flows such as buoyant plumes or jets, emanate from heated surfaces due to density gradients generated by the differences in temperature. The density gradient produces proportional body forces in a gravitational field inducing free convection currents. These flows have been the subject of continuing research.

Spalding and Cruddace [Ref. 9] performed a theoretical analysis for the steady laminar buoyant flow above a line heat source. Their analysis was followed by Fujii [Ref. 10] who also studied the flow above a point heat source. Forstrom and Sparrow [Ref. 11] applied these analyses to experiments they performed above a heated wire. They observed plume

oscillations and determined the transition and onset of turbulence in terms of a modified Grashof number.

A study of the transition of plane plumes was conducted by Bill and Gebhart [Ref. 12]. Their investigation in air clarified some of the mechanisms involved in the transition to turbulent buoyant flow. Evaluating not only quantitative data, but also visual criteria from interferograms, they identified the effects of disturbances in the transition process and were able to define the limits of the transition regime in air.

C. PRESENT STUDY

The present study continued the investigation of natural convection heat transfer from a flush mounted heater on a larger horizontal substrate in water begun by Hickey [Ref. 8]. The primary focus was on the buoyant plume emanating from the surface. While previous studies involved point, line, or horizontal finite sources, little is known about free boundary flow from a finite source surrounded by an unheated area such as a substrate mounted electric component.

The objectives of this study were:

- To fabricate a traversing thermocouple probe and to use the probe to measure the temperature distribution within the buoyant plume.
- To investigate meandering motions of the plume reported in earlier studies.
- To investigate the transition of the free boundary flow above the heat source.

- To visualize the buoyant flow above the surface in order to interpret the meandering and transition process of the flow.

II. EXPERIMENTAL APPARATUS AND PROCEDURES

A. EXPERIMENTAL APPARATUS

The experimental apparatus consisted of four primary interrelated systems and two independent secondary systems as seen in Figure 1. The primary systems included: the power supply system; the test surface heater system; the thermocouple probe traversing system; and, the data acquisition and reduction system. The secondary systems included: the flow visualization system and the water deaeration and filtering system. The power supplied to the heater, the temperature measurements on the test surface and in the buoyant plume, the position of the thermocouple probe, and the temperature of the ambient fluid, are the related variables of the primary systems that the experiment depended upon. Flow visualization and water deaeration/purification were independent systems.

All of the systems mentioned above are described by Gaiser [Ref. 13], Haukenes [Ref. 14], Akdeniz [Ref. 15], Larsen [Ref. 16], and Hickey [Ref. 8]; described are the basic set-up, the water tank, data acquisition system, and water filtration system, and additions or modifications such as the deaeration system or the thermocouple traverse system. The following

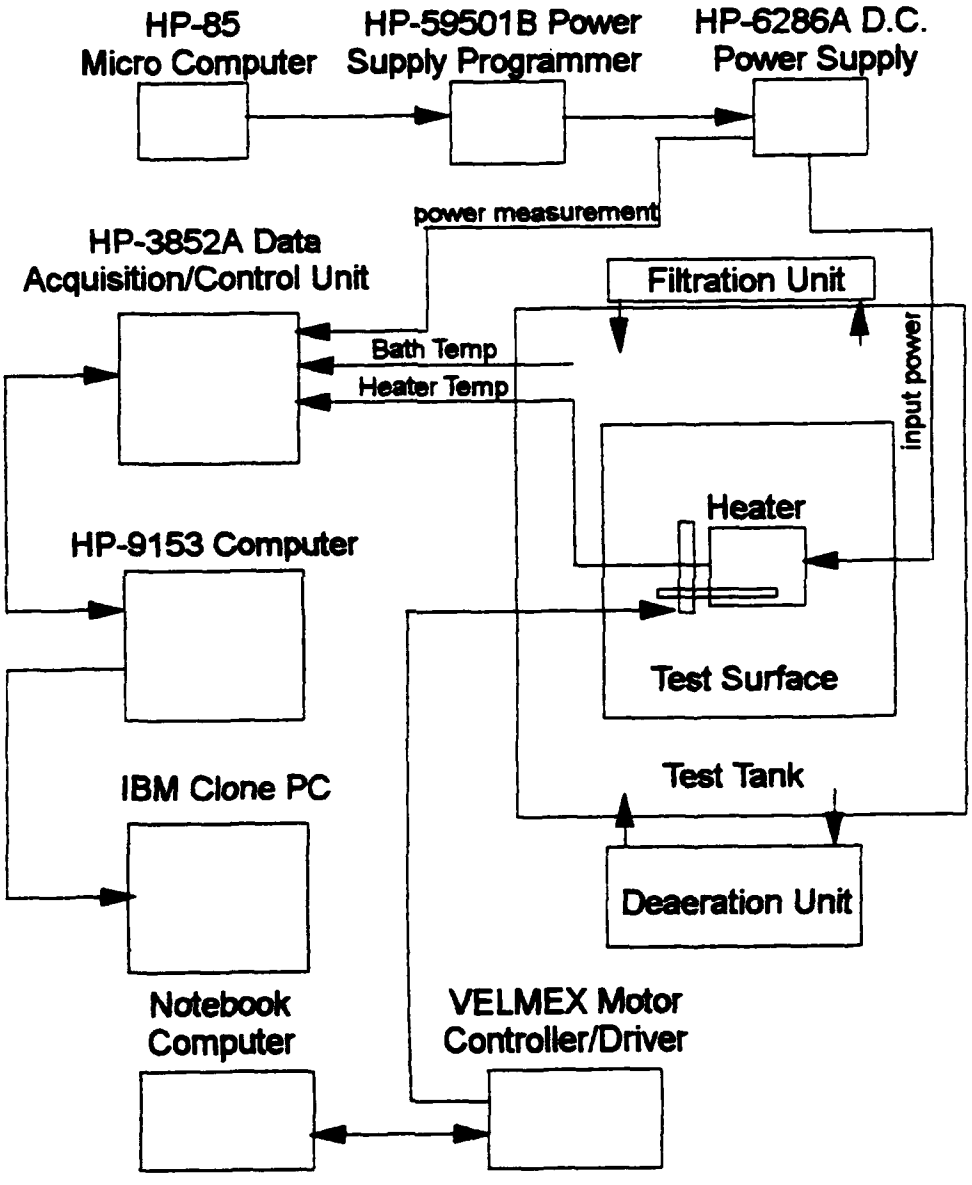

Figure 1. Top View of the Experimental Apparatus.

summarizes those systems and describes modifications which reflect the current condition of the apparatus.

1. Test Surface

The test surface was described in detail by Hickey [Ref. 8]. The surface consisted of a 30.48 cm x 30.48 cm horizontal substrate with a 9 cm x 9 cm heater flush mounted in the center. Embedded in the surface, under the heater, were twenty-five 0.013 cm copper-constantan thermocouples as seen in Figure 2. The heater, which provided a uniform heat

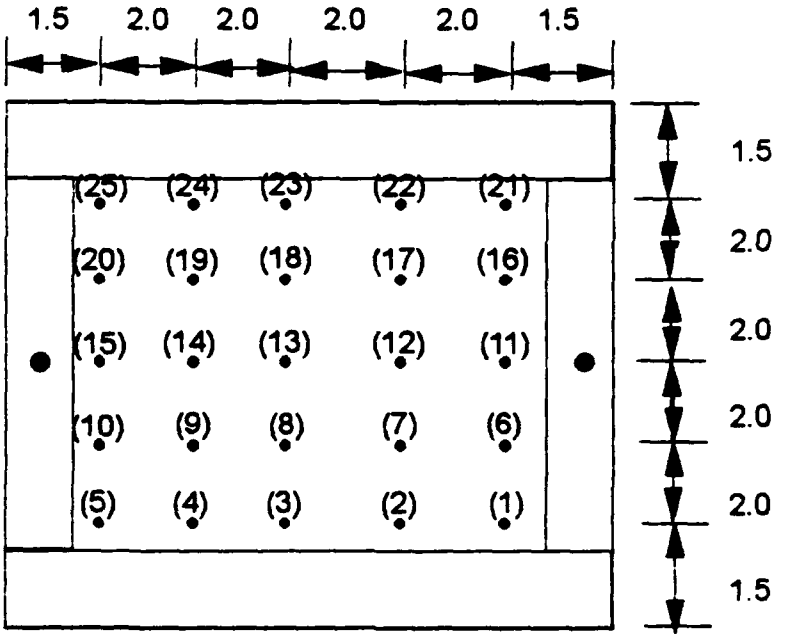

Figure 2. Thermocouple Locations under Test Heater.

flux, was a gold/tin oxide film with a surface resistance of 2.6 ohms/square; net thickness of film and substrate was 0.165 mm. The film was attached above the thermocouples using a thermally conductive epoxy. The power leads were attached to

the film using a silver loaded "ink" with a resistance of 0.2 ohms/square. When the power leads were attached, the entire surface had a resistance of approximately 3 ohms. Covering the entire test surface was a thermochromic liquid crystal (TLC) sheet. Used to ensure a smooth flat surface, the sheet also provided a visualization of the temperature patterns on the surface; it was calibrated in water and showed: yellow at approximately 41°C, green at 43°C, blue-green at 45°C, and dark blue at temperatures above 47°C.

Because the thermal properties of the various components of the test surface were different, care had to be taken when increasing the power to the heater because sudden thermal expansion would cause it to fail. This occurred when the gold/tin oxide film heater was rapidly heated and conduction to the substrate was slow; the gold/tin oxide would separate from the film upon which it was attached because of the bonding power of the epoxy. Reattachment of a new gold/tin oxide heater proved difficult after failure occurred and required slight modification of the surface.

The difficulty in rebuilding the test surface was with the attachment of the power leads to the new gold/tin oxide film. The original surface was built from the top down and attachment of the power leads to the gold/tin oxide film prior to affixing the film to the surface was possible. In the latter case, the power leads could only be affixed simultaneously with attachment of the film to the substrate.

Because the loose wires of the power leads were difficult to work with, copper strips were soldered to the power leads, and the strips embedded in the substrate as seen in Figure 3.

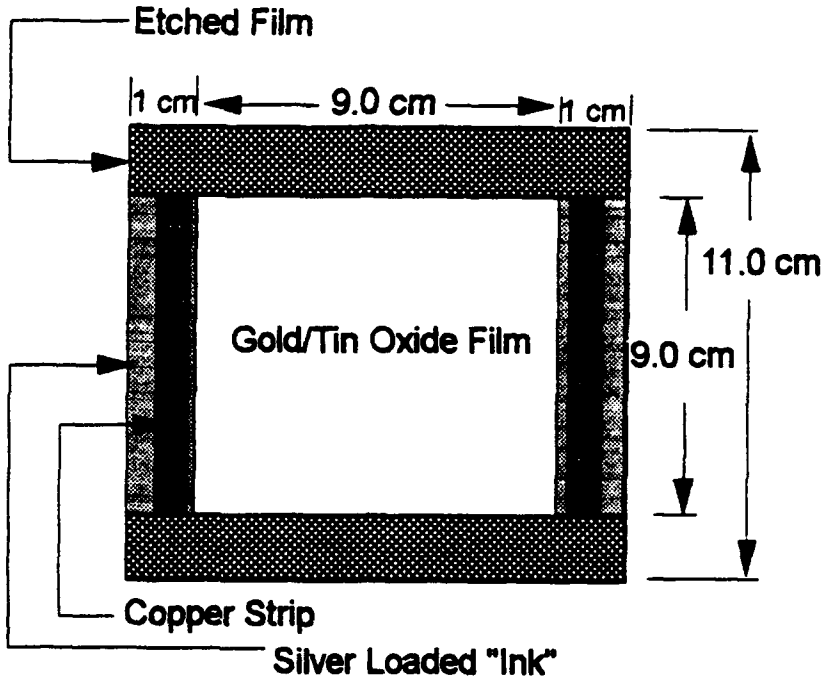

Figure 3. Bottom View of Test Heater.

With a solid conductive strip, the gold/tin oxide film could easily be attached to the surface by spreading the epoxy on the substrate, the silver loaded "ink" on the copper strips, and pressing the film in place. The result was that a 3 ohm surface resistance was easily obtained across the rebuilt heater.

2. Power Supply System

The entire experiment is driven by the power supply system which provided the power to the test surface heater. The driver in this system was a HP-85 micro computer which was programmed to control various power inputs to the test surface heater. The computer directed a HP-59501B Isolated DAC/Power Supply Programmer, which in turn controlled the HP-6286A D.C. Power Supply that actually provide the power to the heater. As shown in Figure 4, the heater was connected in series with

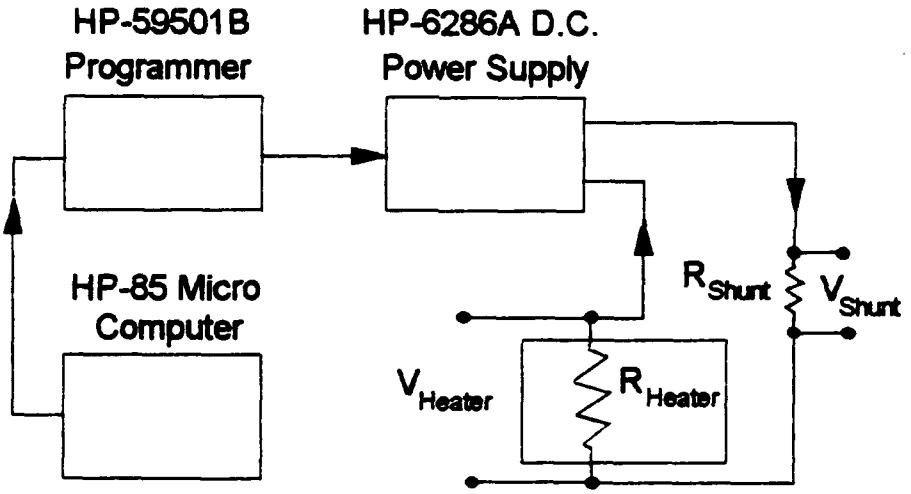

Figure 4. Power Supply System.

a 0.101 Ohm precision shunt. By obtaining the voltage across the precision shunt (V_{shunt}) and across the heater (V_{heater}), and by knowing the resistance through the precision shunt (R_{shunt}), the input power to the surface can be computed using the following equation:

$$Power = \left(\frac{V_{shunt}}{R_{shunt}}\right) V_{heater}$$

3. Thermocouple Probe Traversing System

The thermocouple probe traversing system was used to obtain temperature measurements at specific locations in the buoyant plume. The system consisted of a thermocouple probe, a traversing system with three degrees of freedom, and a IBM PC clone "notebook" computer.

The thermocouple probe was made by passing the ends of 0.0076 mm copper-constantan thermocouple through two bent glass capillaries which were bonded together. The ends of the 0.0076 mm thermocouple wires were then welded to 0.76 mm wire. The 0.76 mm wires and glass capillaries were then pulled through a stainless steel tube, bonded in place, and the ends of all the tubes were sealed. The probe, shown in Figure 5, was then attached to the traverse via a stainless steel rod.

The traversing slides, manufactured by VELMEX, consisted of two motor driven slides and one manually positioned slide. The powered slides were positioned by a 86MM-2 two axis stepping motor controller/driver. These were used to move the probe within a horizontal plane according to position commands entered into the "notebook" computer. The manual slide, with a 30 cm vernier scale, was used to move the probe in specific planes above the heater surface. The entire

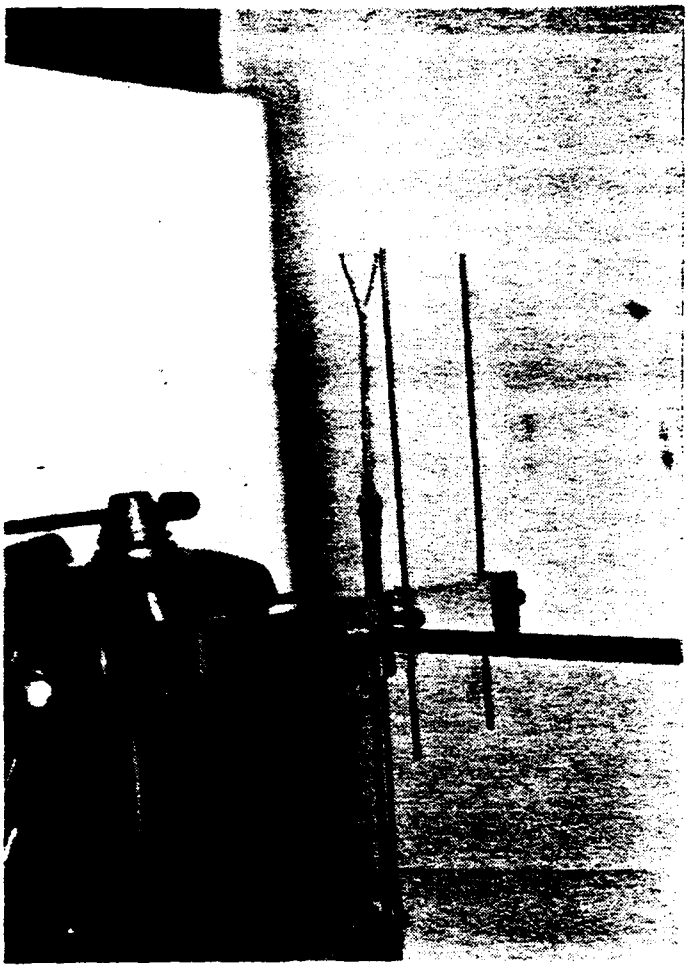

Figure 5. Thermocouple Probe.

system was mounted above the water tank directly over the heater test surface.

4. Data Acquisition/Reduction System

The data acquisition/reduction system was completely described by Larsen [Ref. 16]. It consisted of a HP-9153 computer, a HP-3852A Data Acquisition/Control Unit, and an IBM

clone personal computer. The HP computer was programmed to interrogate the data acquisition unit for monitored temperature and voltage measurements, and to transmit the reduced information to the IBM clone via an export program. The IBM clone was used to process the imported data through spreadsheet and graphics programs.

5. Secondary Systems

Not directly linked to the four primary systems, the flow visualization and deaeration/filtration systems were considered secondary. The flow visualization system consisted simply of a He-Ne laser whose beam was spread into a sheet through a cylindrical lens to illuminate suspended particles in the water. As seen in Figure 6, a SLR camera was used to

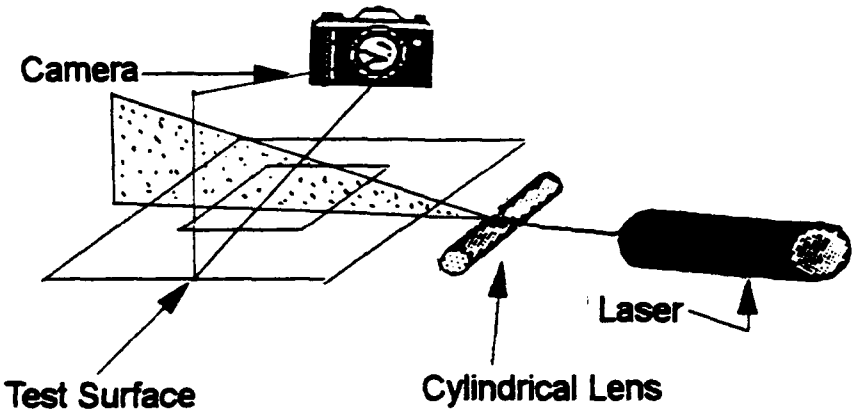

Figure 6. Flow Visualization System.

photograph the flow path of the particles through the buoyant plume as they passed along the sheet of generated laser light.

The deaerating unit consisted of a deaerating tank, a vacuum pump, a heater, and a discharge pump. With the vacuum pump lowering the pressure in the deaerating tank to 68 to 85 kPa, water was suctioned into the tank through spray nozzles. With the pressure low and the heater increasing water temperature, entrained air escapes from the water as it settles into the tank. The deaerated water is then returned to the test tank via the discharge pump. Attached to the deaerating unit return line is the filtration unit. This unit suctions water from the test tank and passes it through four cartridge filters which remove particulates and deionize the water.[Ref. 13]

B. EXPERIMENTAL PROCEDURE

The experimental program consisted of three phases: test surface temperature evaluation, buoyant plume temperature evaluation, and visualization of the buoyant flow. In preparing for all phases, a mechanical mixer was operated for at least five minutes to dissipate temperature stratification within the test tank. All primary systems were then activated while the tank was permitted to reach quiescence, which took approximately 30 minutes.

1. Test Surface Temperature Evaluation

The procedure for evaluation of the test surface was completely described by Hickey [Ref. 8]. Power was provided to the test heater. After approximately 15 minutes, when steady state was reached, temperature measurements were taken on the surface of the heater over a nine minute period. This was done for seven different constant and two different periodic power levels.

2. Buoyant Plume Temperature Measurements

Following the surface temperature measurements for a specific power level, temperature measurements in the buoyant plume were obtained. Measurements were obtained within one quadrant over the heater surface at nine locations and six elevations.

To obtain the plume temperature measurements, the thermocouple probe was used. Measurements always commenced with the probe in the center position (45 mm,45 mm) at an elevation of 2.0 mm above the surface. At that position, the data acquisition program was run and 1300 temperature measurements were obtained over a period of 260 seconds. Early evaluation of the data acquisition program and measurements showed that a 5 Hz sampling frequency was adequate to meet Nyquist sampling criterion.

When plume temperature measurements at one position were obtained, the probe was repositioned. This was

accomplished by typing movement instructions on the "notebook" computer which relayed these instructions to the controller/driver and caused the traverse slides to move to the new position. After the plume was given time to settle following disturbance by probe positioning, the above procedures were repeated until readings were obtained for the nine positions at six different elevations.

3. Flow Visualization

The final phase of the experiment program involved flow visualization. With all temperature measurements obtained, contamination of the test tank with the flow visualization particles was possible.

With the test heater powered at specific levels, ground pliolite powder was dispersed in the test tank. These particles are easily suspended in the water (specific gravity 1.026) and scatter laser light when illuminated. A vertical plane of laser generated light was passed over the center of the test heater to illuminate the particles which could then be photographed at extended time exposures. Photographs were taken for 15, 30, 60, and 120 second exposure times at a low, medium, and high input power. The procedure was described in detail by Gaiser [Ref. 13].

III. ANALYSIS OF FLOW VISUALIZATION

Flow visualization was conducted for a number of input powers. The objective was to obtain representative flow patterns for a low, medium, and high heater power level. Results for five different power levels, of which one was also the average of a pulsatile triangular wave input power, were successfully obtained. Photographs were taken of two perpendicular central planes above the test surface.

The focus of the flow visualization program was to verify some of the reports made in earlier studies. Forstrom and Sparrow [Ref. 11] observed that for purely laminar flow the plume exhibited slow, regular meandering motion. They also noted that depending on the heating rate and elevation above the source the onset of transition was indicated by turbulent bursts. Bill and Gebhart [Ref. 12] observed the effects of disturbances in aiding the onset of transition.

All the photographs were taken with various exposure times in the range 15 to 120 seconds. Because of that, the flow paths of the suspended particles were represented by streaks during the period the particles were within the illuminated sheet; in this study the streaks made were referred to as "pathlines."

A. LOW POWER OBSERVATIONS

The low power observation was made at a 3.2 W power level, corresponding to a heat flux of 395 W/m^2. At this low power, as seen in Figure 7, it was clear that meandering of the plume was taking place. In the top photo the plume flow is to the right and seems to remain steady for the one minute exposure time. The bottom photo, taken seconds later and exposed for two minutes, shows the plume shifted towards the left. In this photo some particles are still flowing to the right and would indicate that the flow to the left was not quite steady. The second plane observations at this power level were similar.

Particles in both planes seemed to follow distinct paths except when the plume would shift while meandering. In the plume base pathline crossing was not evident and would indicate that flow at this low power was laminar.

Observations at a slightly higher power level of 7.1 W (877 W/m^2) showed a distinct flow vertically upward with no meandering of the plume. It was clear from the visualization that particles were still following pathlines that did not cross. Hence, flow was assumed to be laminar.

B. MEDIUM POWER OBSERVATIONS

Observations at medium power levels showed characteristics of departure from laminar flow. Photographs were taken at power levels of 11.4 W (1407 W/m^2) and 19.8 W (2445 W/m^2).

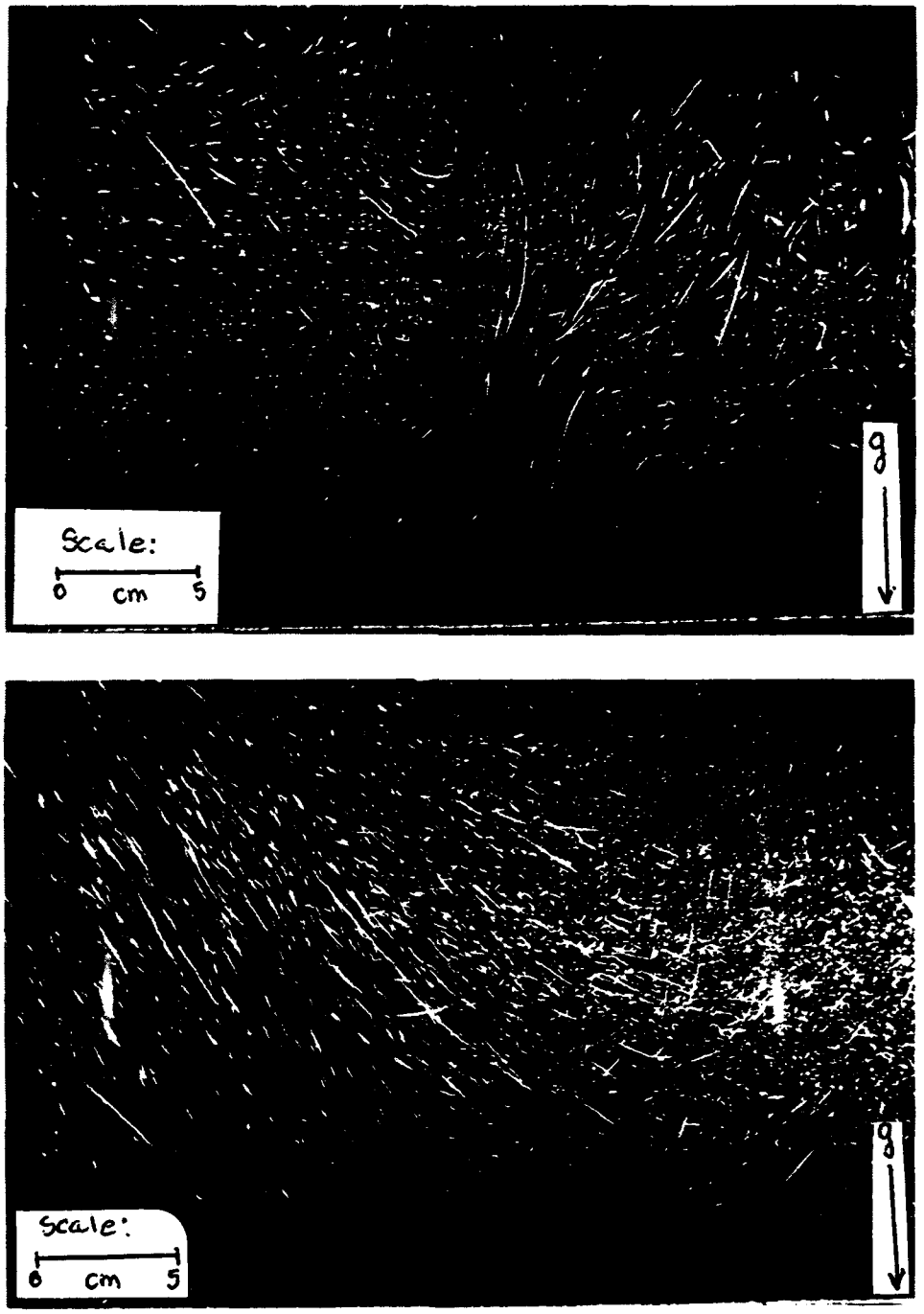

Figure 7. Buoyant Plume at Low Power (3.2 W) (top) 60 second exposure time (bottom) 120 second exposure time.

Observations were also made for a pulsatile input power using a triangular wave pattern with an average power of 19.8 W, 0.1 Hz frequency, and 8 W amplitude.

Photographs taken for the nominally steady power inputs clearly showed evidence of a well defined buoyant plume with no evidence of large meandering as seen at lower power levels. As seen in Figure 8 for 19.8 W (2445 W/m^2) power level, effects of time dependence are observed in the form of crossing of the particle paths.

Use of a pulsatile input power did not show a pronounced effect on the buoyant plume. The flow pattern for a 19.8 W steady input power was not significantly different from that at the 19.8 W average, pulsed power input. Pathlines for both power inputs, as shown in Figure 8, are quite similar within the plume. However, outside the plume, the effect of the power pulsation at this low frequency appears to cause a downward flow towards the heated surface prior to entrainment in the plume. The plume width is also seen to be larger in the presence of pulsations. This is obvious in the bottom photograph. Because this was the only case where a pulsatile power was used, no explanation for this effect is possible.

Also evident in the photographs for medium power levels was a slight narrowing of the plume compared to the lower input power. The higher power level causes an increase in fluid velocity and a thinner thermal and momentum transport

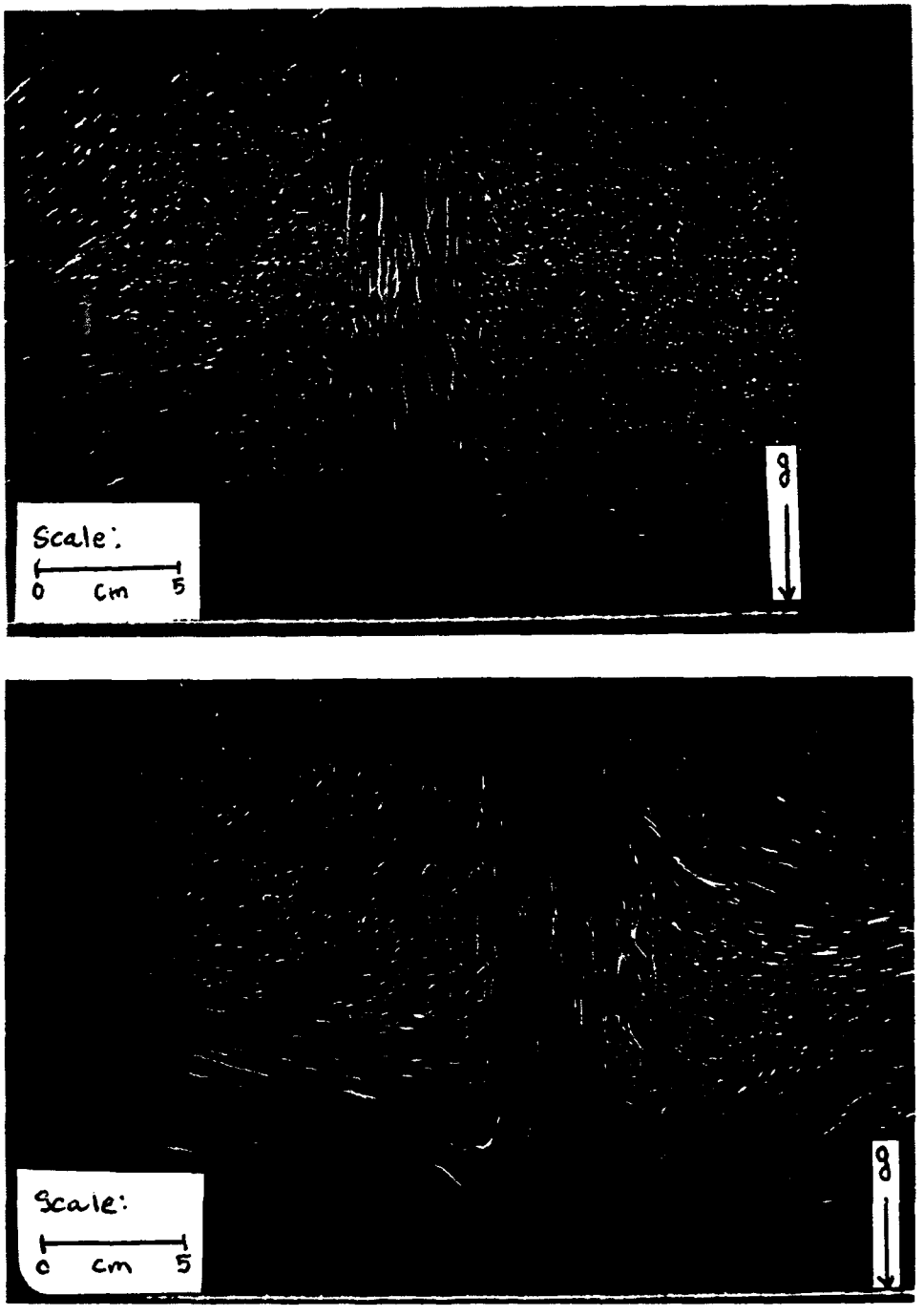

Figure 8. Buoyant Plume Medium Power (19.8 W - 60 second exposure time) (top) steady (bottom) pulsatile.

region. That, coupled with the appearance of crossing of particle paths indicates a transition to turbulent flow.

C. HIGH POWER OBSERVATIONS

Observation of the buoyant flow at high power was made at 48.9 W. From the photograph in Figure 9, a further narrowing of the plume is apparent. Closer to the surface, pathlines appear to cross much more than in the photographs at lower powers. Entrainment of particles from the sides along the free boundary is more evident. Flow at this power input appears to be in transition or turbulent conditions evidenced by the mixing in the field of view of Figure 9.

Figure 9. Buoyant Plume at High Power (48.9 W - 60 second exposure time).

IV. ANALYSIS OF PLUME TEMPERATURE DATA

Plume temperature measurements were processed in two ways. First, the temperature difference data were plotted as time series graphs as shown in Figure 10. The x,y, and z coordinates of the spatial location are identified at the upper right corner. A total of 54 measurements were taken at each power level. A Fast Fourier Transform (FFT) was performed to better identify the frequency components of the temperature signal obtained by the thermocouple probe over 1024 data points. Data were initially taken at a 15 Hz sampling frequency which revealed that the maximum frequency observed was approximately 0.2 Hz. Therefore, the sampling frequency was set at 5 Hz, in excess of Nyquist sampling criterion, in order to avoid aliasing. The power spectral density (PSD), a measurement of the energy of the signal at various frequencies, was then obtained. The frequencies (in Hz) defined by the FFT were then plotted against PSD (a non-dimensional magnitude), also shown in Figure 10.

Data were obtained for seven constant power and two periodic power inputs. After reviewing the plots described above, the data were divided into three categories: low, medium, and high power. Next, all the data were reviewed together in order to determine group trends. Because neither the time series plots, nor the FFT plots revealed significant

differences between constant power inputs and the periodic power input with the same mean, periodic power inputs will not be discussed.

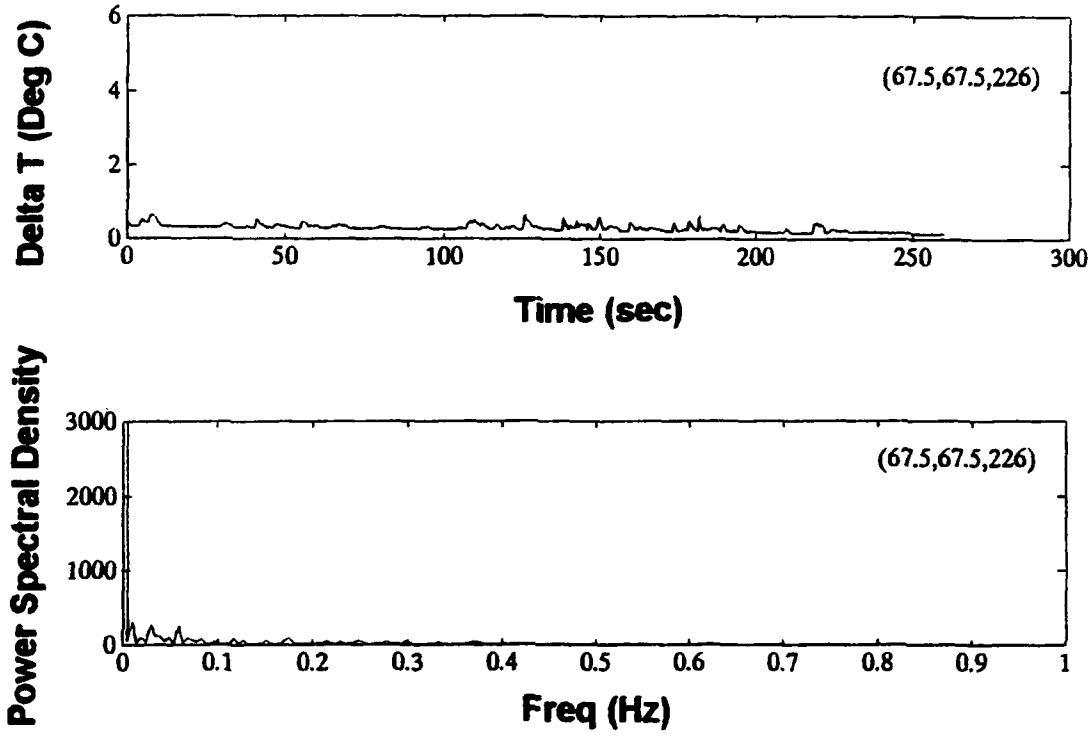

Figure 10. Example of Time Series and FFT/PSD Plots.

A. LOW POWER OBSERVATIONS

Data in the low power regime were obtained at 0.78 W (96 W/m^2) and 3.2 W (395 W/m^2). The time series plots for the 0.78 W power level shown in Figure 11 reveal low frequency, small amplitude oscillations close to the surface, and are nearly constant at all other elevations. Seen in Figure 12, the FFT plots at this power level show only a few peaks with small PSD

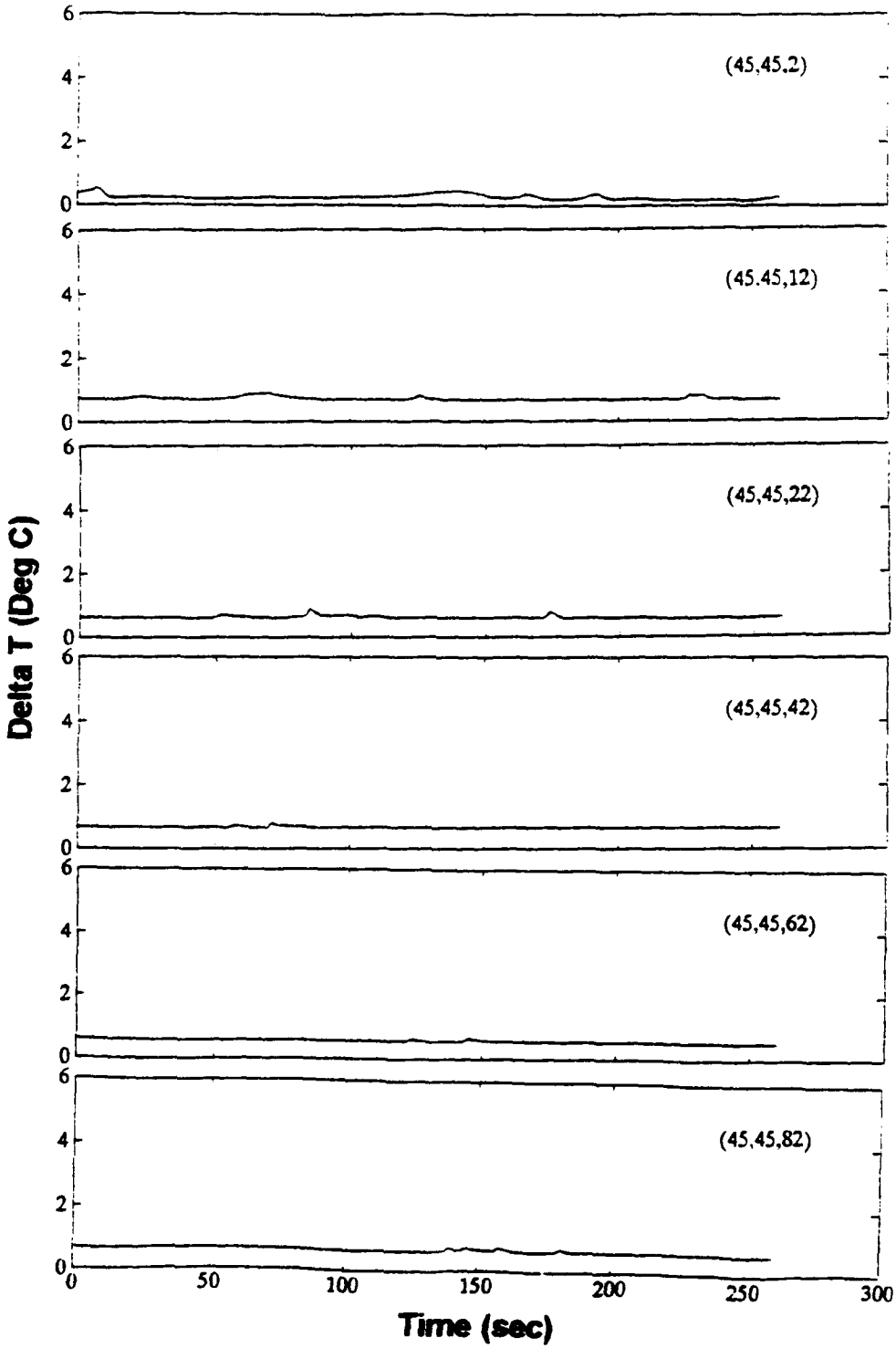

Figure 11. Time Series along Plume Centerline at 0.78 W.

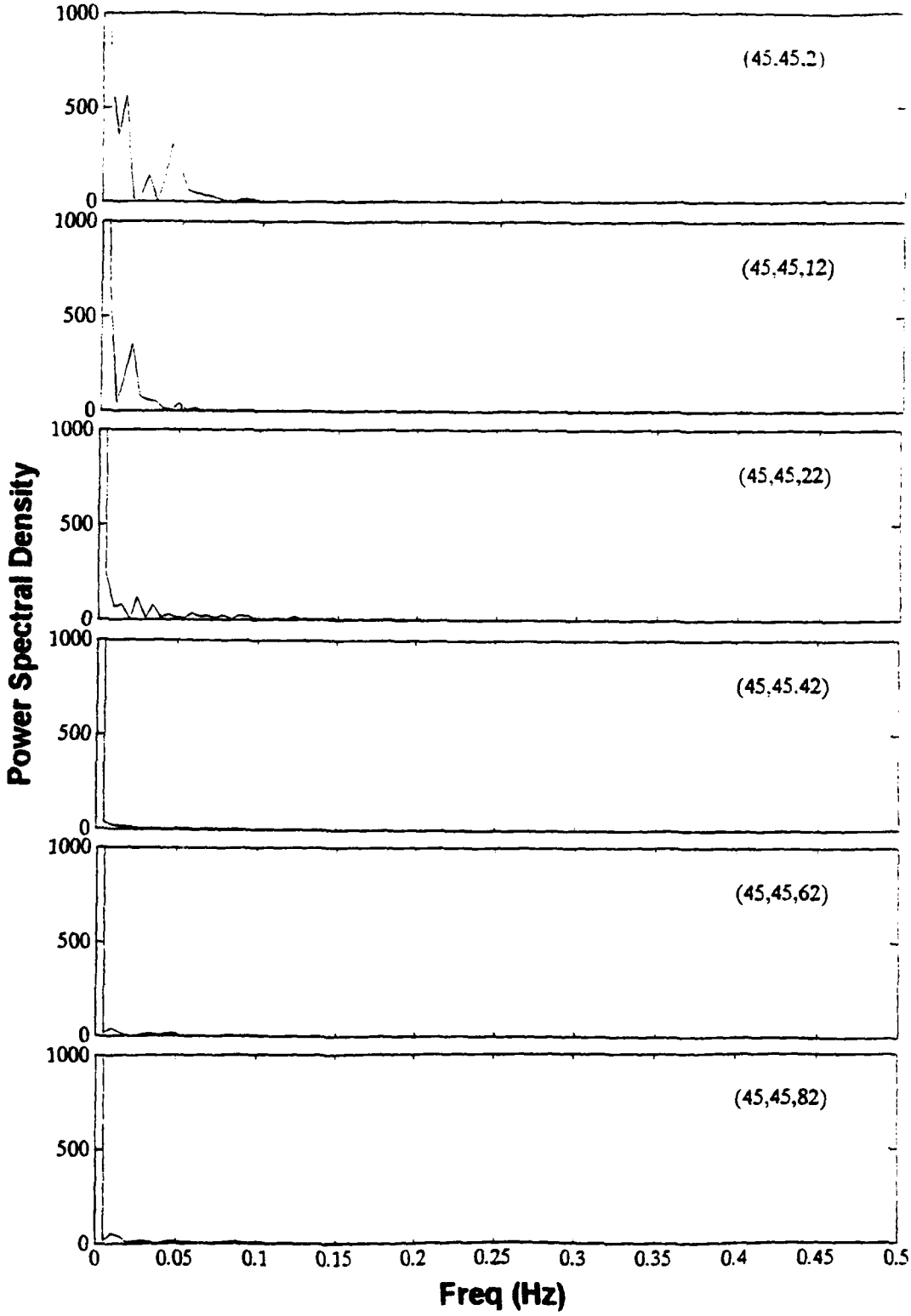

Figure 12. FFT/PSD along Plume Centerline at 0.78 W.

magnitudes at very low frequency. Clearly, buoyant flow at this power level at all elevations is laminar.

At the 3.2 W power level the patterns begin to change. Near the surface, the time series plot shows an increase in the frequency of oscillation with larger amplitude. As the elevations increase, the dominant frequency of oscillation increases, and the amplitude decreases. See Figures 13 and 14. The FFT plots reveal that near the surface, more frequencies are evident with much higher energy. As elevation increases, more frequencies are apparent, but with lower energy. At the lower elevations, the buoyant flow is clearly laminar. But as elevation increases, it is believed that the flow is undergoing transition as discussed in more detail later.

B. MEDIUM POWER OBSERVATIONS

Two input powers were considered to be in a medium regime because both the time series and FFT plots showed trends that were noticeably different from both those of the low and high power regimes. Medium regime data were obtained at 12.2 W (1506 W/m^2) and 19.8 W (2445 W/m^2). For both power levels, time series plots showed a marked increase in amplitude and frequency of oscillation of delta T near the surface. The FFT plots revealed peaks which were much more defined and over a broader range of frequencies. The energy levels at the defined frequencies also increased.

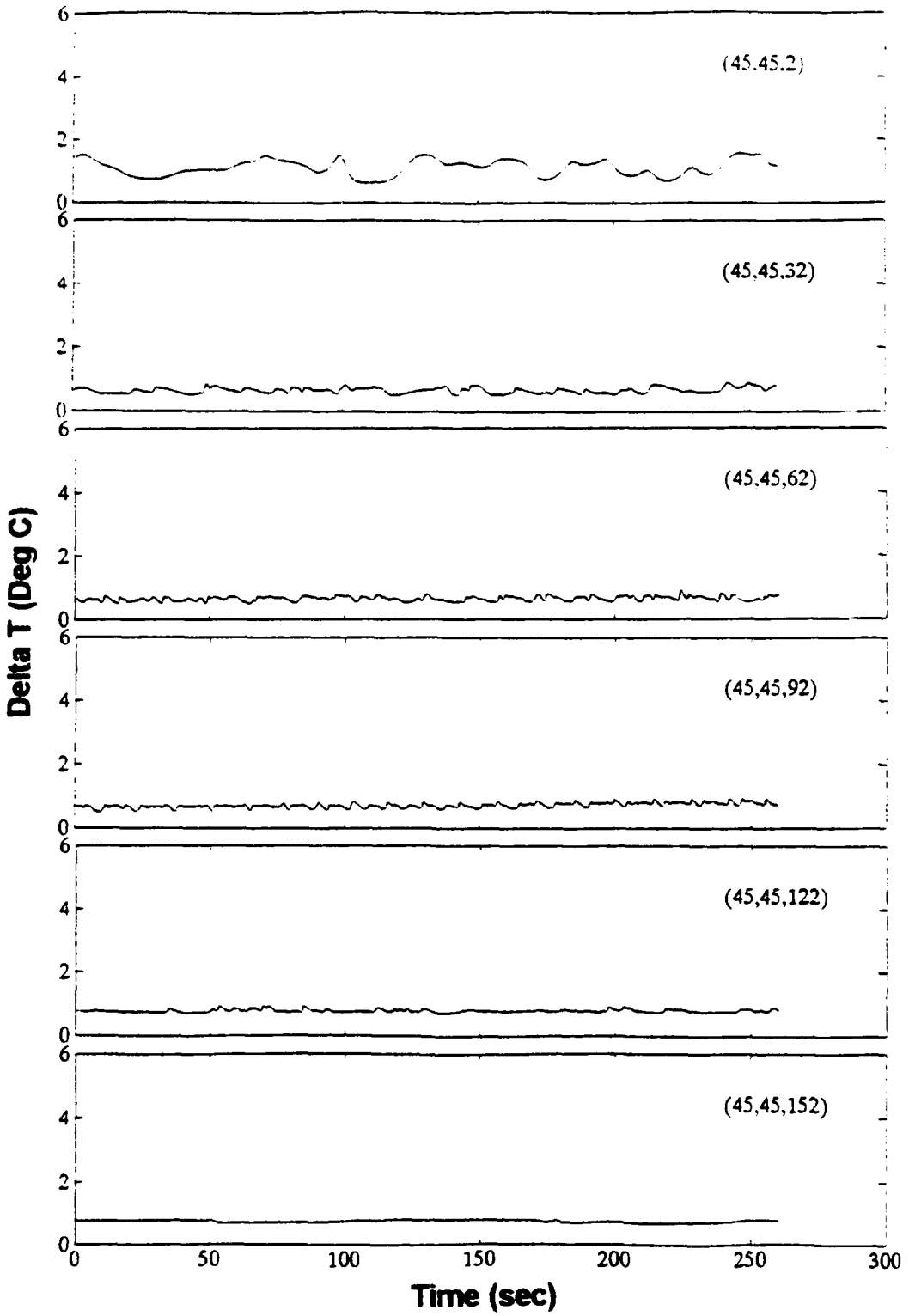

Figure 13. Time Series along Plume Centerline at 3.2 W.

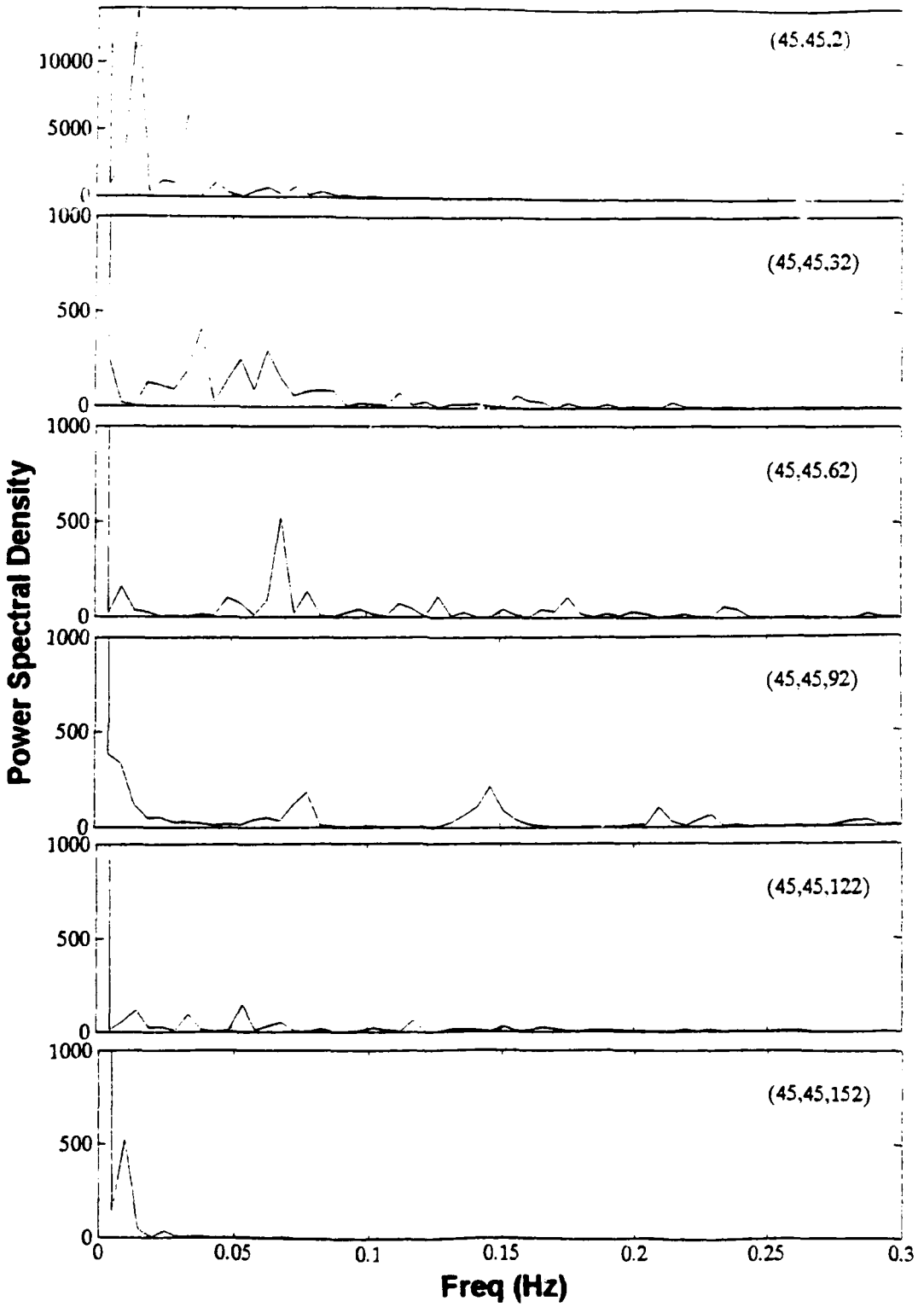

Figure 14. FFT/PSD along Plume Centerline at 3.2 W.

In spite of the similarities mentioned above, differences between the 12.2 W and 19.8 W power levels were also obvious. See Figures 15 to 18. The time series plots at 12.2 W had smaller amplitude oscillations as compared to the 19.8 W input power. More noticeable, was the difference in the FFT plots. At 19.8 W, many more frequencies were identified, with much higher energy levels. It is believed that flow near the surface at 12.2 W is laminar, while transitioning at all other levels, never becoming fully turbulent. The broad range of frequencies that are evident in the FFT plots at 19.8 W seems to indicate that the flow at the two elevations near the surface is in transition, as shown by the high-energy low-frequency peaks, but is near turbulent at higher elevations where more lower energy frequencies become apparent. As was seen in the (67.5,67.5) location plots at 19.8 W, a broad range of frequencies is still evident. This implies that the buoyant plume has not yet narrowed, an indication of turbulent flow evidenced at the high power levels in flow visualization.

C. HIGH POWER OBSERVATIONS

Three power levels were considered to be in the high power regime: 27.8 W (3432 W/m^2), 37.7 W (4654 W/m^2), and 48.9 W (6037 W/m^2). At all three power levels the buoyant plumes have narrowed. This is clear from the FFT plots at the off centerline positions. Of the three power levels, at elevations above the surface, only the 32 mm elevation at 37.7

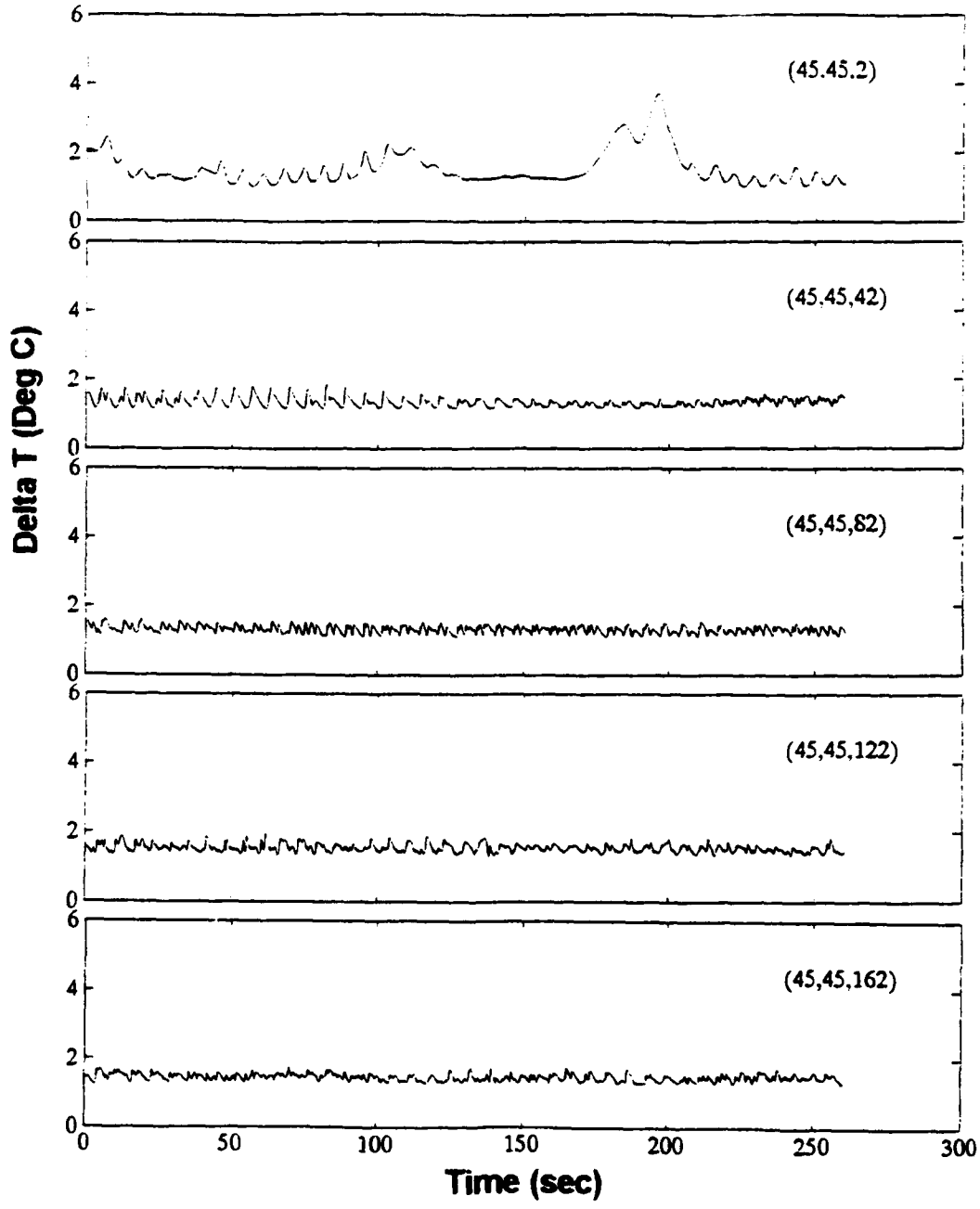

Figure 15. Time Series along Plume Centerline at 12.2 W.

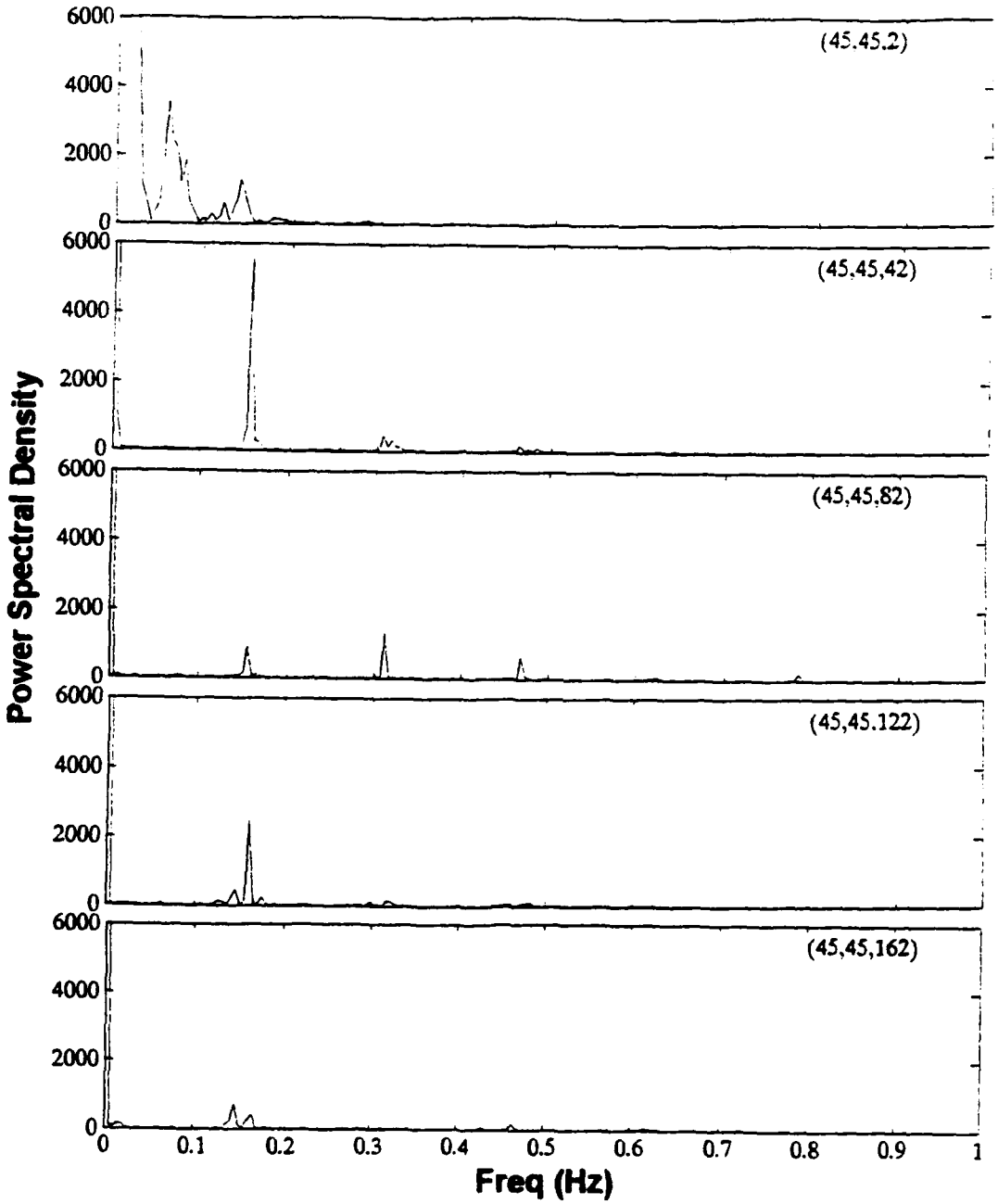

Figure 16. FFT/PSD along Plume Centerline at 12.2 W.

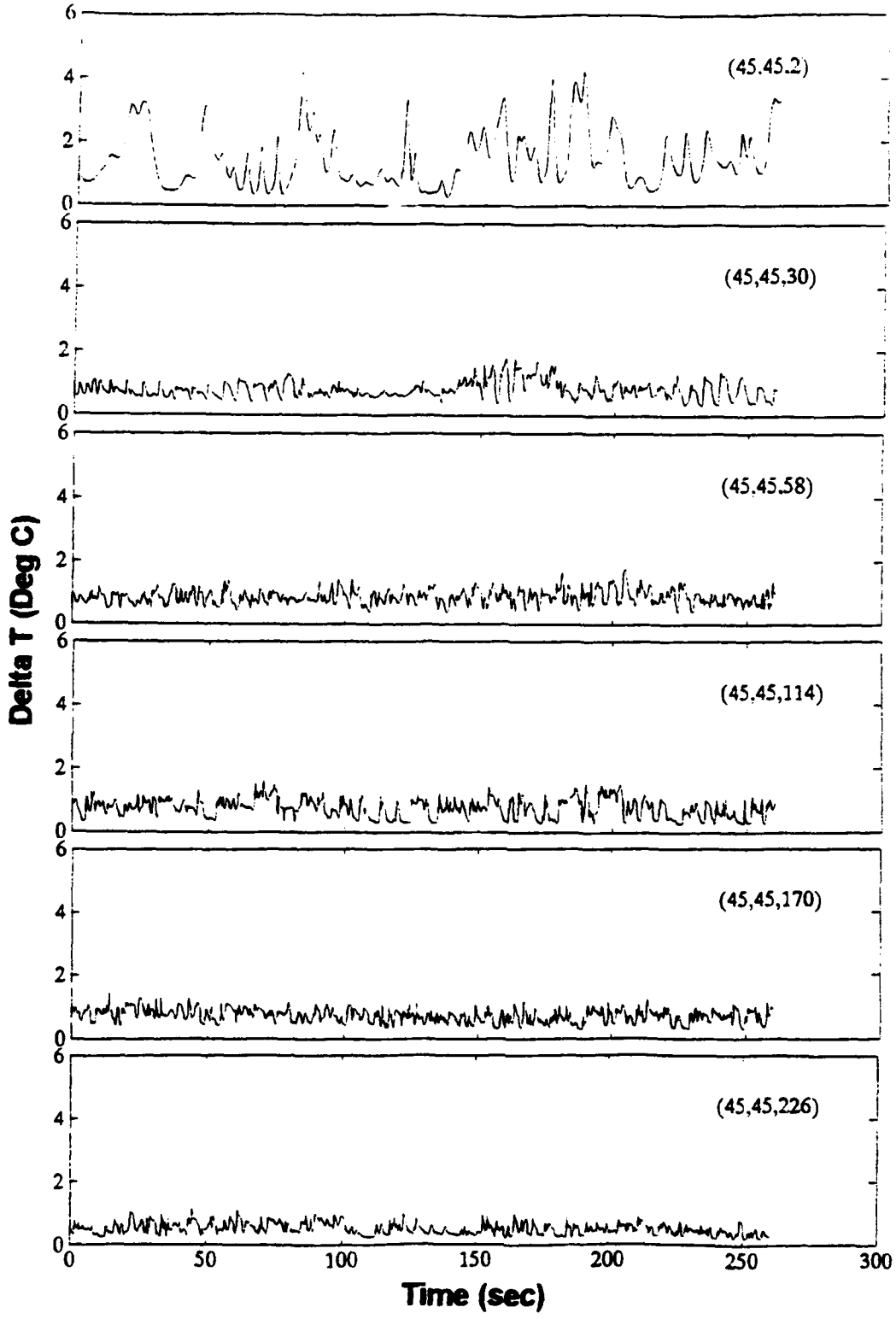

Figure 17. Time Series along Plume Centerline at 19.8 W.

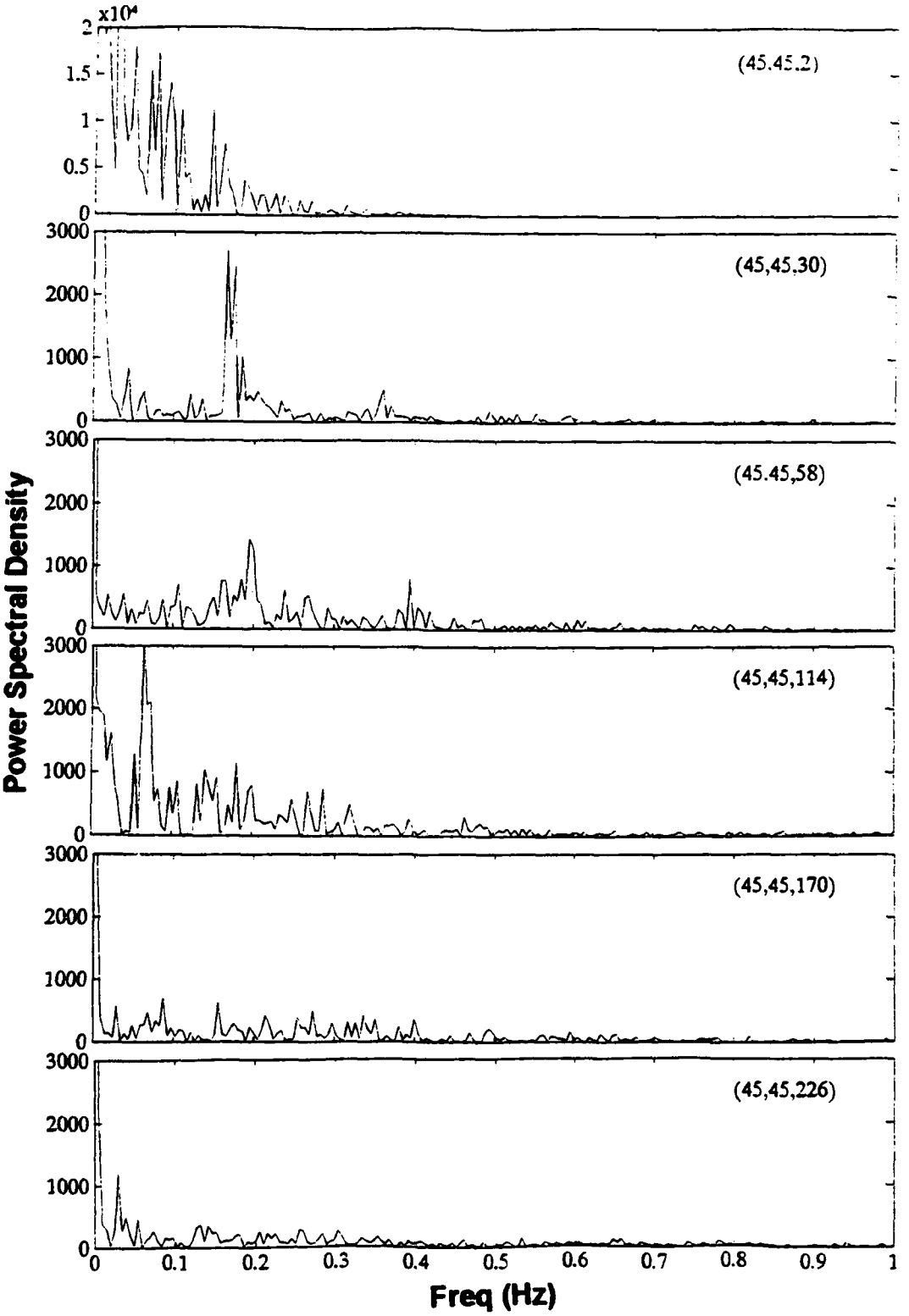

Figure 18. FFT/PSD along Plume Centerline at 19.8 W.

W resulted in a noticeable signal. The time series plots at these power levels show a nearly constant delta T over the period of observation.

At the plume centerline position, time series plots as well as the FFT plots for the position just above the test surface, show a trend that would be considered to be transition. This is clear from the FFT plots which show a variety of low frequencies at very high energy. At the higher elevations, the plots would indicate that the flow is transitioning to full turbulent flow as the elevations increase. At all power levels higher-energy frequencies are evident over the broadest spectrum. See Figures 19 to 24.

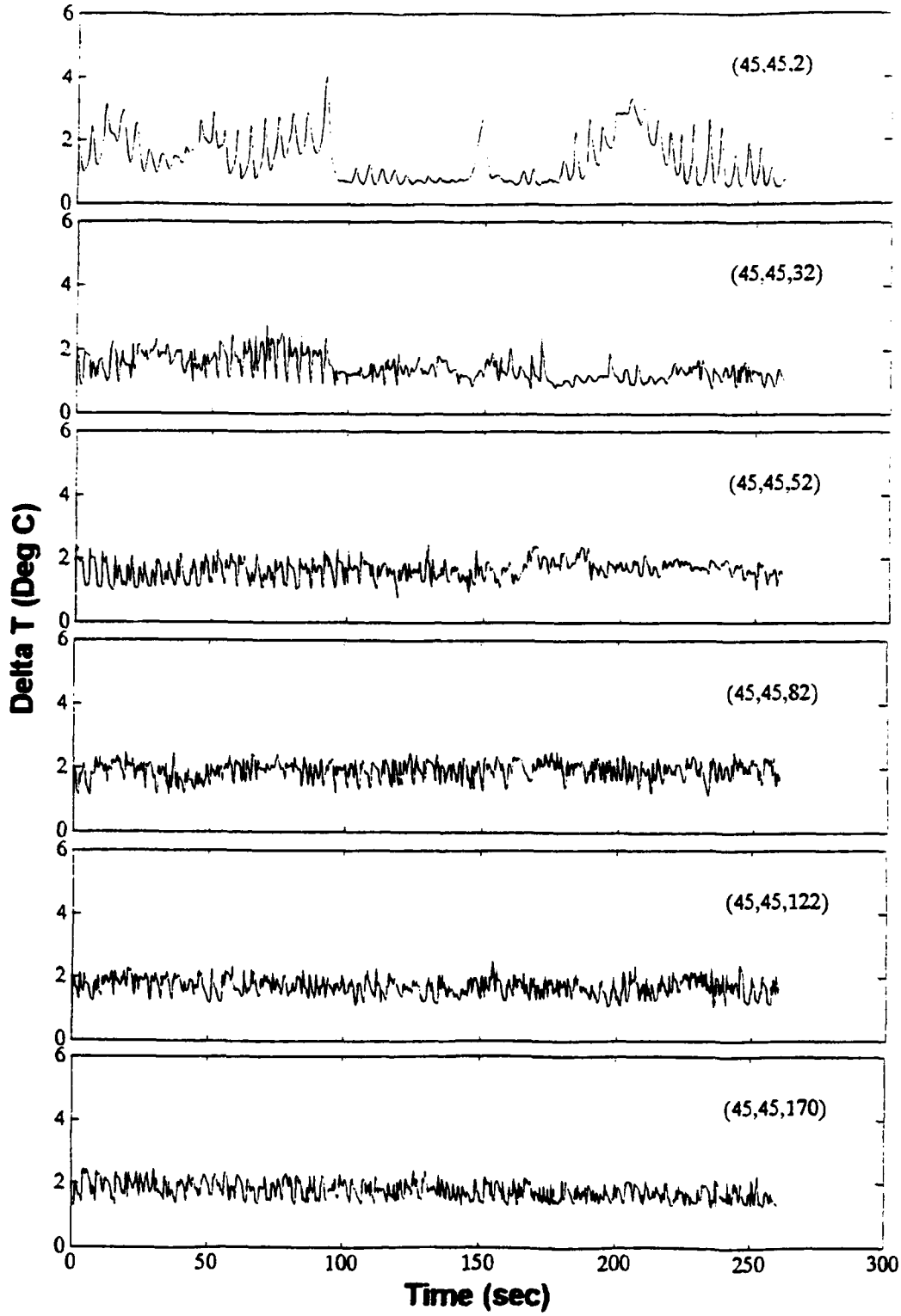

Figure 19. Time Series along Plume Centerline at 27.8 W.

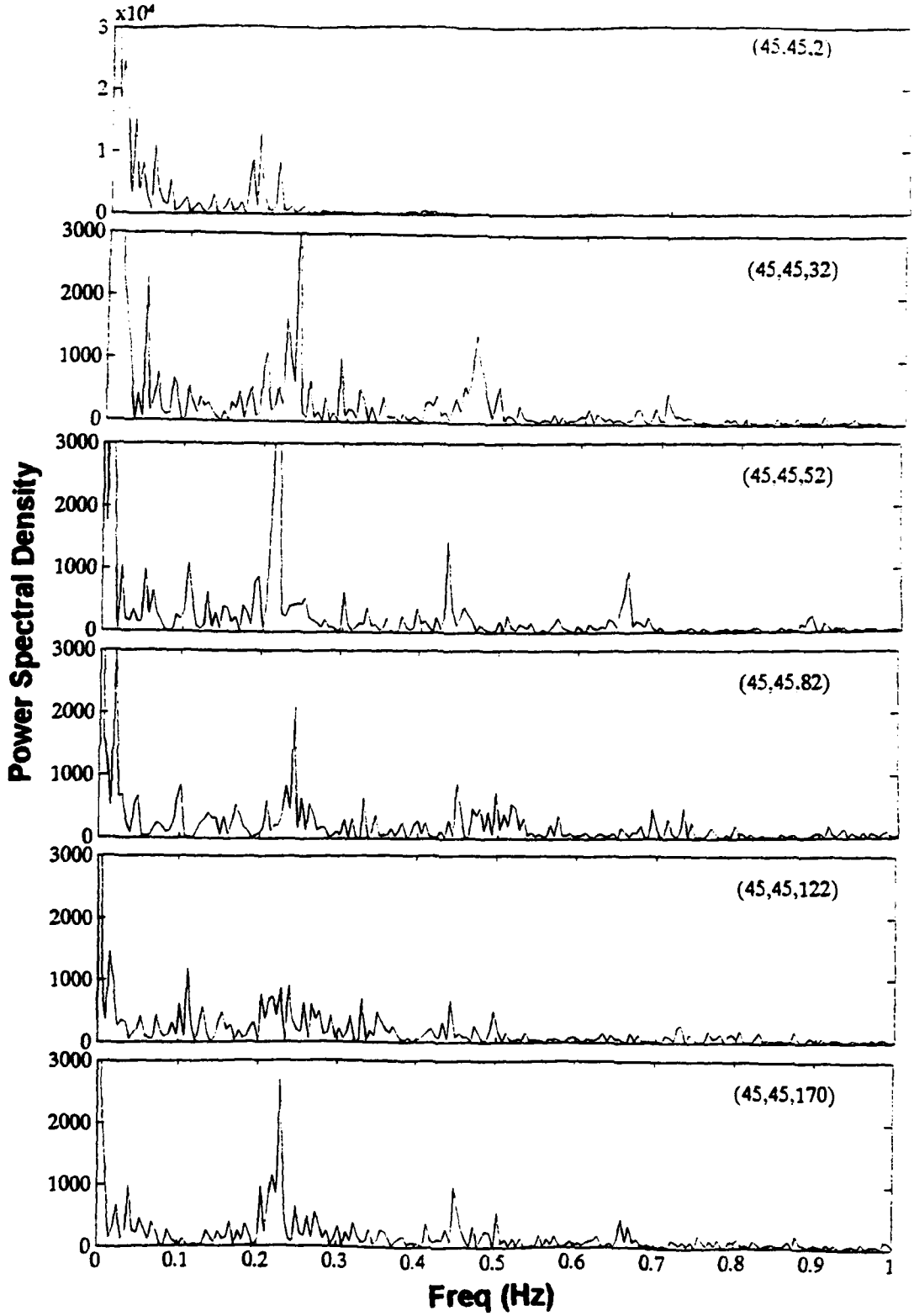

Figure 20. FFT/PSD along Plume Centerline at 27.8 W.

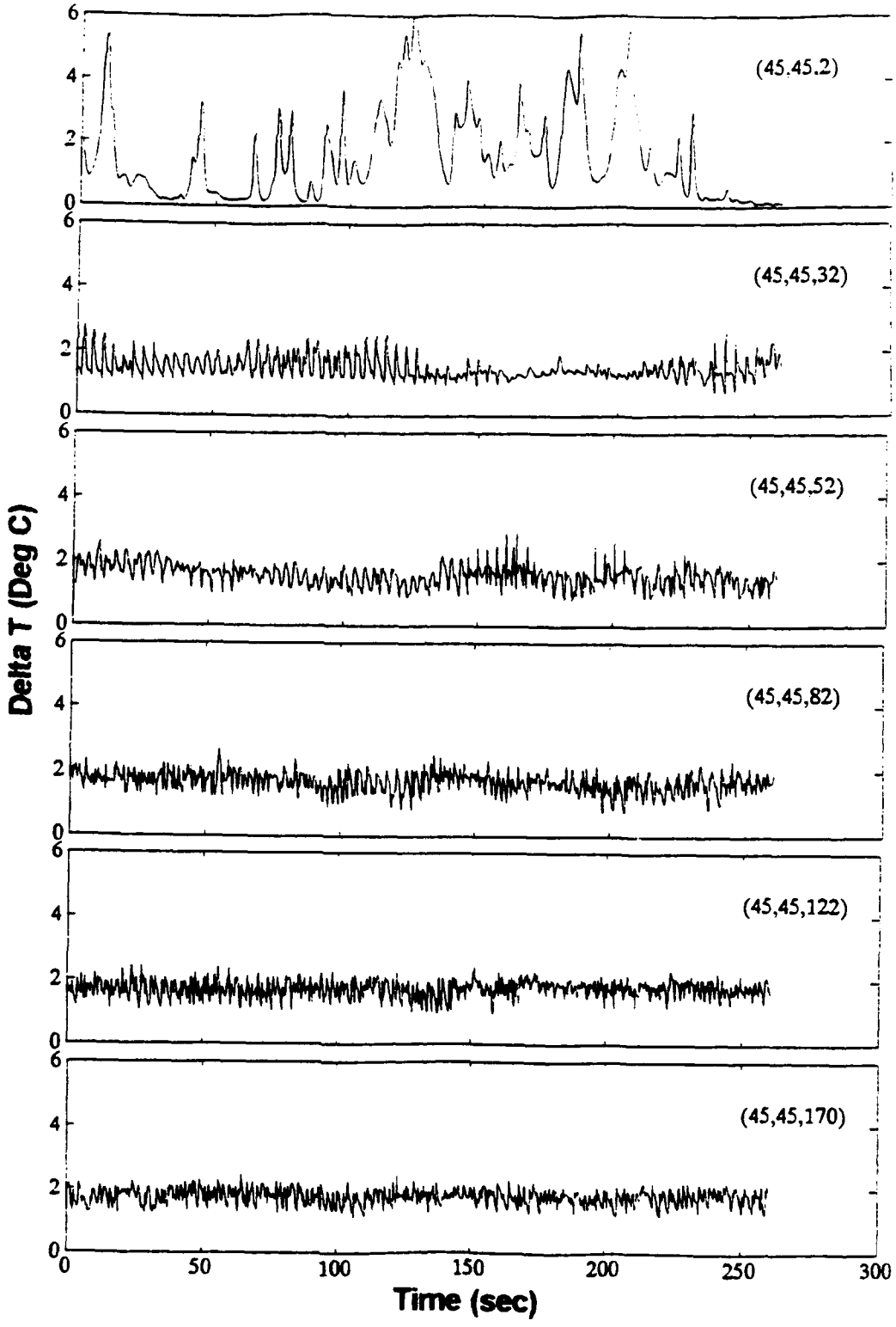

Figure 21. Time Series along Plume Centerline at 37.7 W.

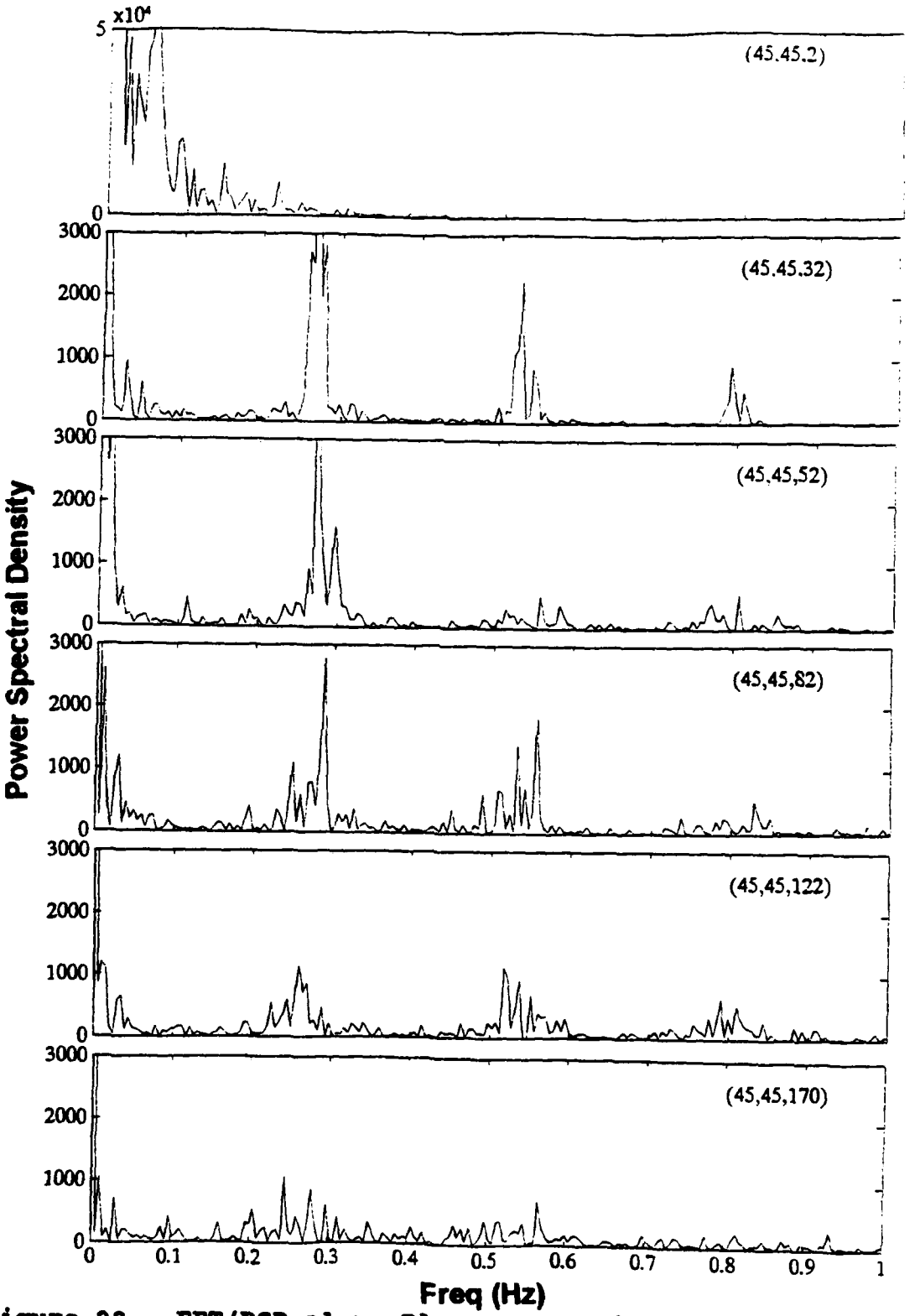

Figure 22. FFT/PSD along Plume Centerline at 37.7 W.

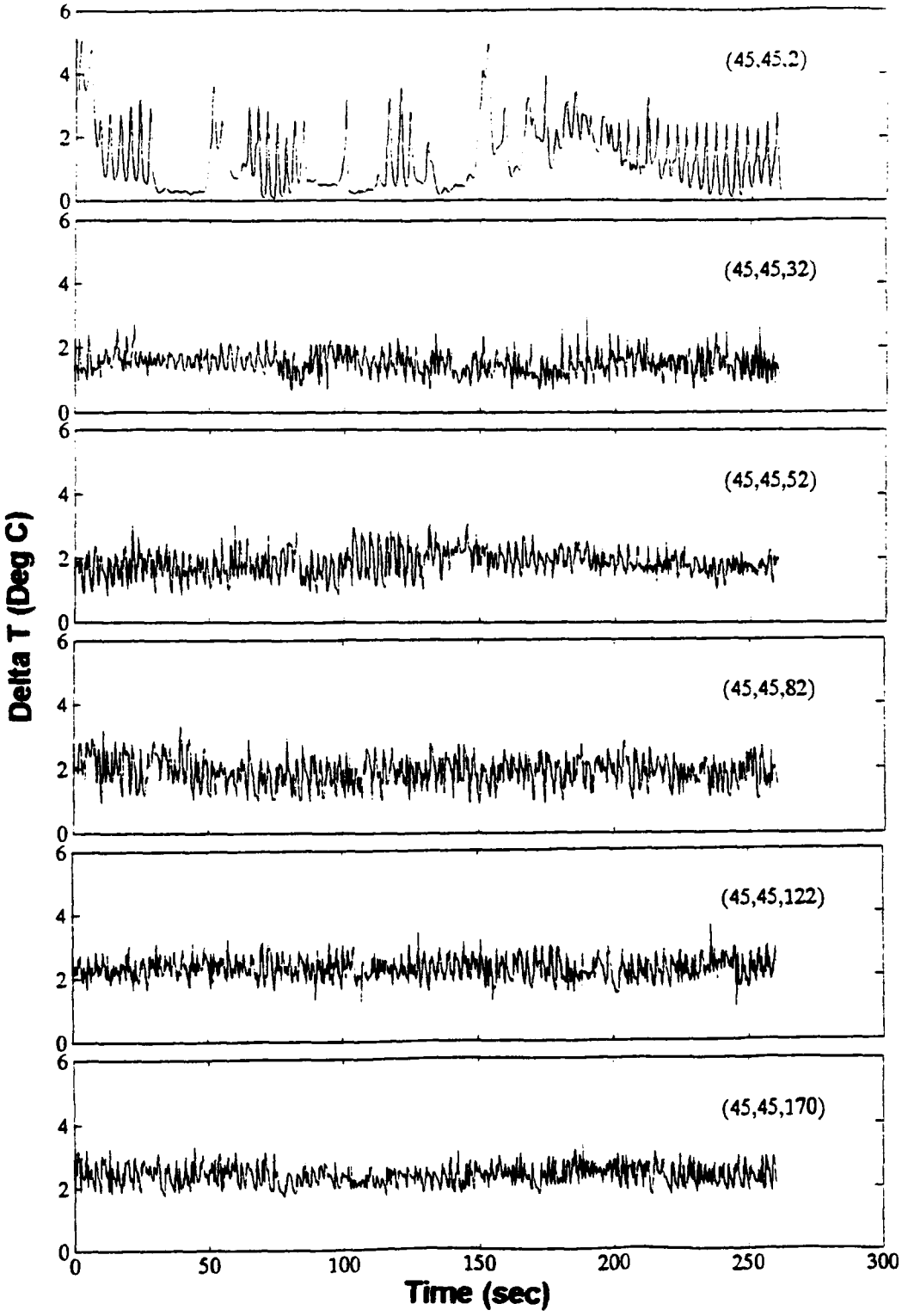

Figure 23. Time Series along Plume Centerline at 48.9 W.

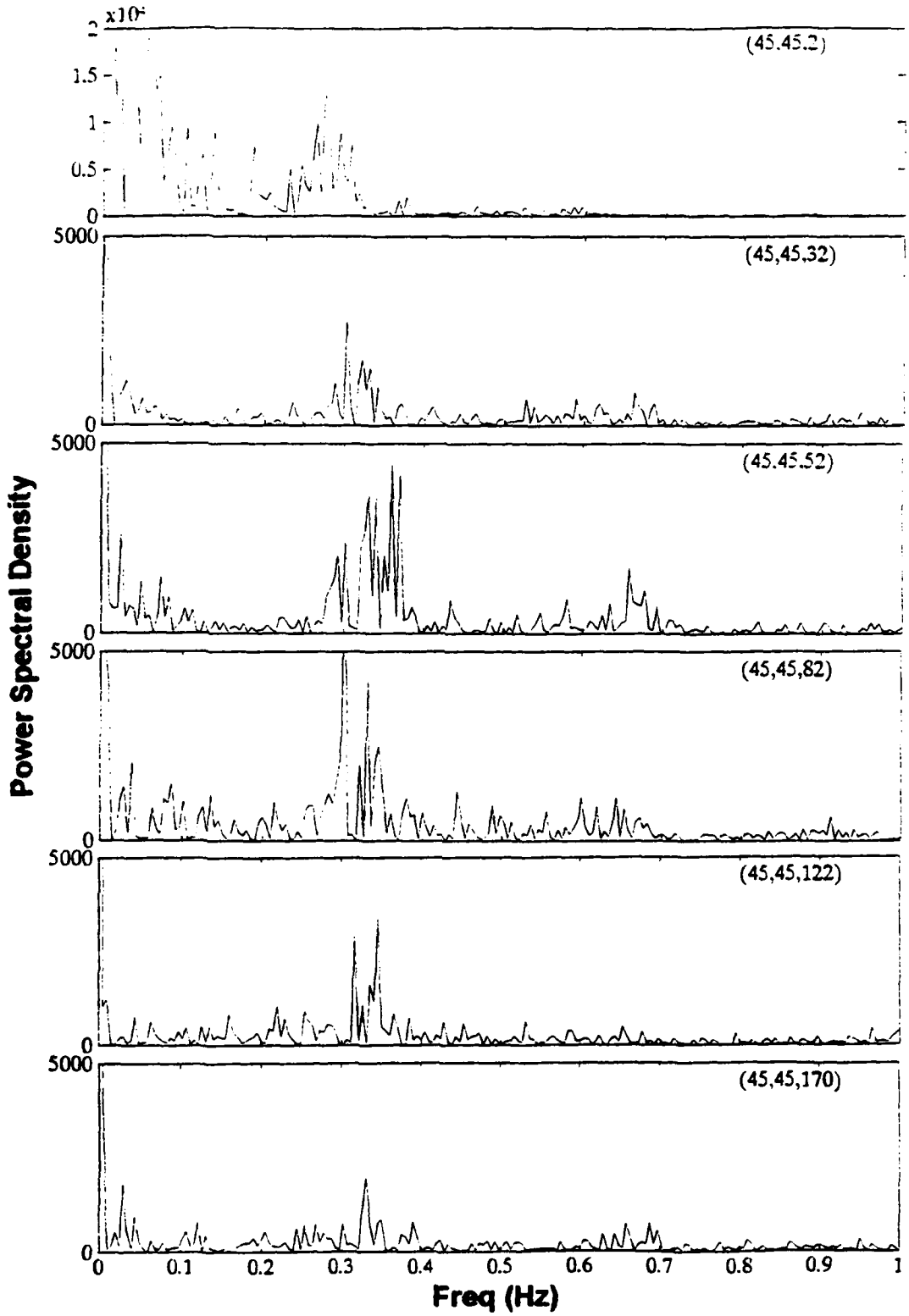

Figure 24. FFT/PSD along Plume Centerline at 48.9 W.

D. COMBINED ANALYSIS

To better evaluate the transition process in the buoyant plume, a single plot was developed which was comprised of data from all the FFT/PSD graphs. Data for the various x,y,z locations in the plume for various heat fluxes are represented. A spreadsheet program was used in the development of the plot, with physical properties of the water taken at a film temperature defined as the average of the mean plate and ambient temperatures, and neglecting conduction heat losses across the bottom of the test surface. An elevation based modified Grashof number:

$$Gr_z^* = \left[\frac{g\beta q'' z^4}{k\nu^2}\right]$$

was plotted against a non-dimensional frequency:

$$f^* = \frac{f}{\left[\frac{g\beta q''}{k}\right]^{1/2}}$$

on a log-log scale as shown in Figure 25. Based on this plot and the observations made from FFT data and flow visualizations, conclusions can be made about the transition process.

The trends of the data points represented in the plot can be characterized in three general areas: $Gr^* < 500$; $500 \leq Gr^* < 1x10^7$; and, $Gr^* \geq 1x10^7$. After evaluating all the graphs

mentioned earlier along with the photographs taken during flow visualization, and in reviewing this final plot, it is concluded that the plot should be divided into four areas which characterize the transition process based on power and

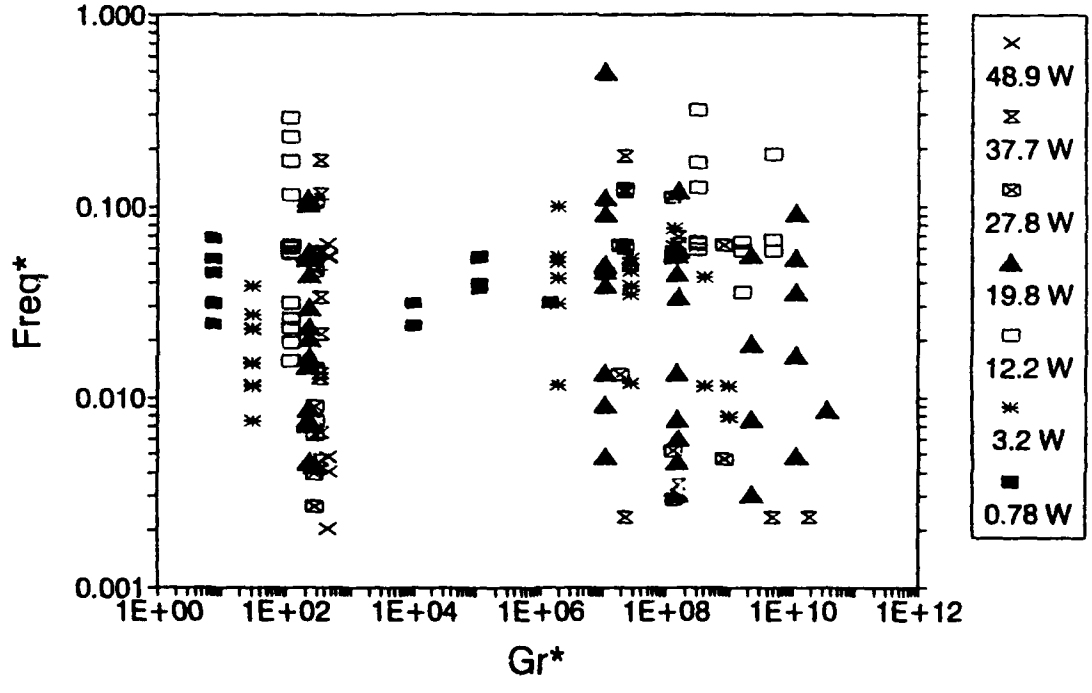

Figure 25. Non-dimensional Frequency versus Grashof Number.

elevation above the surface.

1. Laminar Buoyant Flow Above The Surface

The first region to consider is for Gr* < 500. Data points in this region are for all power levels at an elevation of 2 mm above the surface. As reported by Bill and Gebhart [Ref. 12], spectral analysis of the plume in the laminar region was characterized by high-energy frequencies at the low

end of the spectrum. The reason for the appearance of disturbances is attributed to swaying and oscillations of the plume at its base. This seems to coincide with the FFT/PSD plots obtained.

2. Plume Meandering

For the region $500 \leq Gr^* < 1x10^7$ the buoyant flow above the surface is still laminar but at higher elevations, the plume meanders. Because the motion is a slow movement of the entire plume column, no oscillations are detected in the spectrum analysis. The meandering motion is only evident for low power levels.

3. Plume Transition Region

Transition of the Plume is believed to take place for $1x10^7 \leq Gr^* < 6x10^9$. The beginning point for transition was concluded to be somewhat higher than the values plotted for the 3.2 W power level at the 32 mm elevation. From the photographs obtained at this power level, plume meandering was observed. The end of transition was based on the high end data points for 12.2 W. Clearly from the FFT/PSD plots for the centerline position at this power level, the frequencies represented do not cover a wide spectrum characterizing fully turbulent conditions. Also, the time series plots do not represent a highly oscillating delta T.

4. Turbulent Buoyant Flow

For $Gr^* \geq 6x10^9$ flow is concluded to be turbulent. From FFT/PSD plots of the data points represented by the power levels in this region, frequencies of substantial energy are apparent across a large spectrum. Many data points for the higher power levels were not utilized in Figure 25 because so many distinct frequencies were apparent that the flow was correctly assumed turbulent. Hence, the lack of data points in the turbulent region.

V. TEST SURFACE TEMPERATURE ANALYSIS

A. CONSTANT POWER

Figure 26 shows the heated surface centerline temperature pattern for six of the seven power levels tested. Assuming that conduction losses in the surface are negligible, the

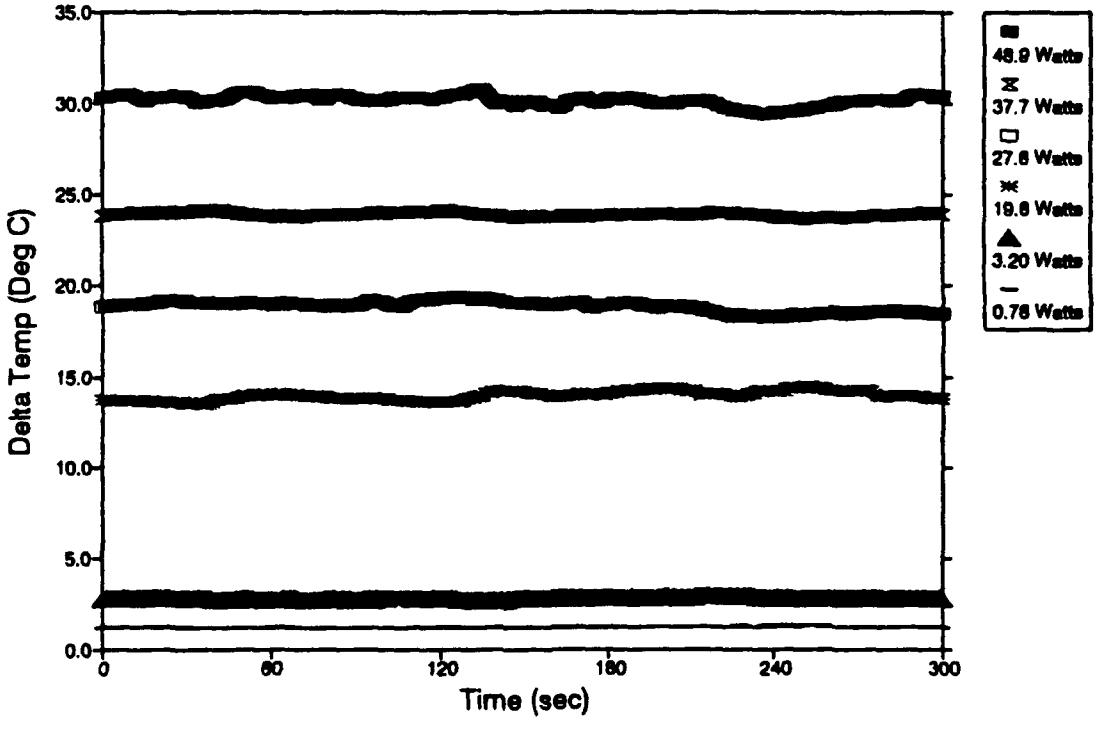

Figure 26. Heater Surface Temperatures at Constant Power.

power supplied to the heater is equal to the heat transferred to the water by convection. Non-dimensional heat transfer data were based on the net heat input rates.

The Nusselt (Nu) and Rayleigh (Ra) numbers were calculated as:

$$N_u = \frac{Q_{Conv} L_c}{kA(T_{plate} - T_{amb})}$$

$$Ra = \frac{g\beta Q_{Conv} L_c^4}{kA\nu^2} Pr$$

Where T_{plate} is the average plate temperature, L_c is a characteristic length taken as the ratio of the heater surface area to perimeter.[Ref. 8]

Having taken all fluid properties at a film temperature defined as the average of the plate and ambient fluid temperatures, a plot of the Nusselt number as a function of flux based Rayleigh number was made. Figure 27 shows a linear best fit of the plotted data which resulted in the following correlation:

$$Nu = 0.135\ Ra^{0.227}$$

valid for $7.5 \times 10^5 < Ra < 8.3 \times 10^7$. This shows a higher exponent of Ra than the correlation determined by Hickey:

$$Nu = 2.22\ Ra^{0.065}$$

which was valid for $1.2 \times 10^6 < Ra < 9.1 \times 10^7$. This could be caused by a greater thermal resistance between the heater and measuring thermocouples in Hickey's data. Evaluation of a temperature based Rayleigh number as defined by Hickey permitted comparison to correlations found by Lloyd and Moran

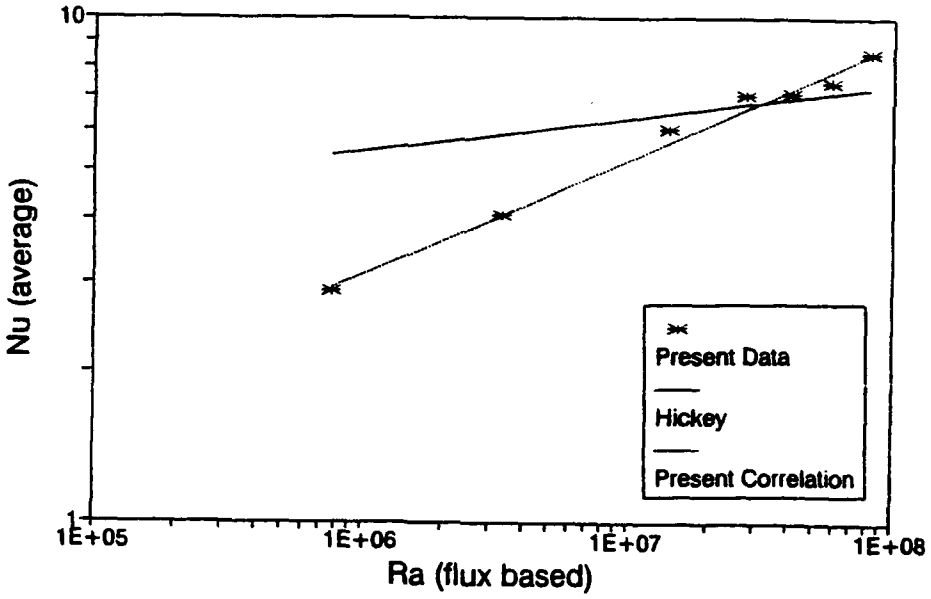

Figure 27. Average Nusselt Number versus Flux Based Rayleigh Number.

[Ref. 4]. A linear best fit of the data in this plot shown in Figure 28 resulted in the following correlation:

$$Nu = 0.08\ Ra^{0.293}$$

valid for $2.6 \times 10^5 < Ra < 9.8 \times 10^6$. As seen in the figure, the slope of the present data agrees with that of Lloyd and Moran but the actual values are considerably lower. Hickey's data are closer but display a lower slope, perhaps due to a higher thermal resistance between the plate and the measuring thermocouples as noted earlier. As pointed out by Hickey, Lloyd and Moran developed their correlations based on a fully heated test surface while the present study has a large unheated low thermal conductivity substrate; which impedes

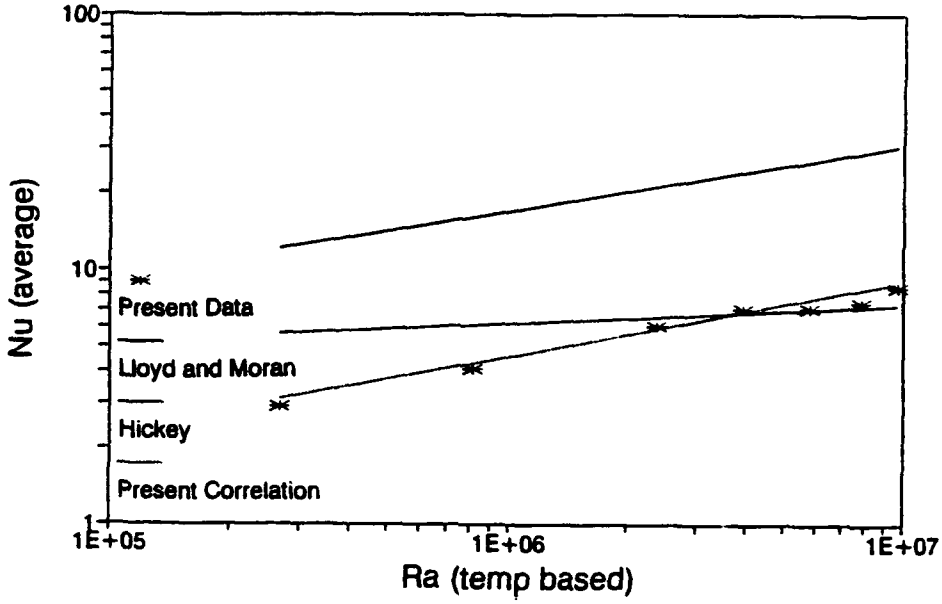

Figure 28. Average Nusselt Number versus Temperature Based Rayleigh Number.

heat transfer near the edges. Also, the fluid used by Lloyd and Moran was air while the present study was based on water and differences in the fluid Prandtl number may effect heat transfer. Lastly, Lloyd and Moran developed separate correlations for laminar and turbulent flow. The correlations developed by Hickey and that of the present study are for the entire range of Rayleigh numbers examined. The correlation developed by Lloyd and Moran for laminar flow had a slope of 0.255 and was valid for $2.6 \times 10^4 < Ra < 8 \times 10^6$ which is in fair agreement with the present study.

B. PERIODIC INPUT POWER

As was described in the previous chapter, the present study showed no apparent benefit in using a periodic input power. Hickey [Ref 8.] noted that for certain types of input powers at specific frequencies, enhancement in the heat transfer from the surface could be obtained. Several attempts were made to repeat results obtained by Hickey, but no significant heat transfer enhancement was noted. From flow visualization it was apparent that the flow was altered by the pulsatile power input. However, too little data was obtained in the present study for pulsatile input powers to verify the heat transfer enhancement findings made by Hickey.

VI. CONCLUSIONS

Use of a traversing thermocouple probe coupled with flow visualization proved invaluable in conceptualizing the flow patterns within a buoyant plume. The temperature measurements obtained by the probe were significant in determining the extent of the plume over the test surface. Flow visualization was vital in verifying the meandering of the plume. Both programs were equally important in understanding the transition process for a free boundary flow above a flat horizontal heated surface surrounded by an unheated area. This can contribute significantly to studies in liquid immersion cooling, particularly in the validation of computational codes.

Use of a pulsatile input power provided no effect in obtaining heat transfer enhancement. The FFT/PSD plots for the pulsatile input powers revealed that the frequency of the input power was buried in the temperature signal obtained. It is believed that the 0.1 Hz input power frequency was too low to affect the plume.

The reconstructed test surface seemed to work as effectively as that built by Hickey [Ref.8]. However, the heat transfer correlations developed from the data obtained from the present surface seemed to be in better agreement with the trends of the previous studies.

VII. RECOMMENDATIONS

While the present study was a continuation of that begun by Hickey [Ref. 8], further research would make the study complete. Therefore, it is recommended that the following aspects be studied further:

- Use the data and results presented in this study to develop analytical models to predict the transition process of buoyant plumes.
- The photographs obtained for through flow visualization were very limited. Flow visualization should be repeated to obtain photographs that clearly show the flow from the test surface as well as at a higher level in the buoyant plume.
- Determine the velocity field in and around the plume using a laser doppler velocimeter to better understand the flow patterns.
- Develop theoretical models which can utilize the results obtained in order to better determine the heat transfer effects on the heater surface.

APPENDIX A

SAMPLE CALCULATIONS

The following calculations were made for a heat flux of 3432 W/m^2, f = 0.425 Hz, ΔT = 17.42°C, and at the elevation z = 0.052 m.

1. **Characteristic Dimensions.**

   Perimeter (P) = 4 x 0.09 m

   = 0.36 m

   Heater Surface Area (A_s) = $(0.09\ m)^2$

   = 0.0081 m^2

   Characteristic Length (L_c) = A_s/P

   = 0.0225 m

2. **Convective Heat Flux.**

   Input Power (Q_{conv}) = 27.8 W

   Heat Flux (q") = 27.8/0.0081

   = 3432 W/m^2

3. **Fluid Properties [Ref. 17].**

   In the plume:

   $\beta = 263.3 \times 10^{-6}\ K^{-1}$

   $\nu = 0.885 \times 10^{-6}\ m^2/s$

   k = 0.611 W/m·K

   Pr = 5.985

On the surface:

$\beta = 334.6 \times 10^{-6}\ K^{-1}$

$\nu = 0.749 \times 10^{-6}\ m^2/s$

$k = 0.623\ W/m \cdot K$

$Pr = 5.00$

4. Non-dimensional Frequency.

$f^* = 0.425/[9.81 \cdot 263.3E\text{-}6 \cdot 3432/0.611]^{1/5}$

$= 0.111$

5. Modified Grashof Number.

$$Gr_z^* = \frac{9.81 \cdot 263.3E\text{-}6 \cdot 3432 \cdot 0.052^4}{0.611 \cdot (0.885E\text{-}6)^2}$$

$Gr_z^* = 1.36x10^8$

6. Nusselt Number.

$Nu = [3432 \cdot 0.0225]/[0.623 \cdot 17.42]$

$= 7.12$

7. Rayleigh Numbers.

Flux based:

$$Ra = \frac{9.81 \cdot 334.6E\text{-}6 \cdot 3432 \cdot 0.0225^4}{0.623 \cdot (0.749E\text{-}6)^2} 5.0$$

$Ra = 4.13x10^7$

Temperature based:

$$Ra = \frac{9.81 \cdot 334.6E\text{-}6 \cdot 17.42 \cdot 0.0225^3}{(0.749E\text{-}6)^2} 5.0$$

$$Ra = 5.8x10^6$$

APPENDIX B

UNCERTAINTY ANALYSIS

The accuracy of the data in this study was determined by performing an uncertainty analysis. For a function comprising a number of independent measurements $F = F(X_A, X_B, X_C)$, the uncertainty of F was calculated as:

$$\delta F = \left[\left(\frac{\partial F}{\partial X_A}\delta X_A\right)^2 + \left(\frac{\partial F}{\partial X_B}\delta X_B\right)^2 + \left(\frac{\partial F}{\partial X_C}\delta X_C\right)^2\right]^{1/2}$$

If the function $F = C\ X_A^a\ X_B^b\ X_C^c$, then the uncertainty is determined by:

$$\frac{\delta F}{F} = \left[\left(a\frac{\delta X_A}{X_A}\right)^2 + \left(b\frac{\delta X_B}{X_B}\right)^2 + \left(c\frac{\delta X_C}{X_C}\right)^2\right]^{1/2}$$

List of properties [Ref. 17]:

$g = 9.81\ m/s^2$

$T_{film} = 298$ K:	$T_{film} = 306.8$ K:
$\beta = 263.3 \times 10^{-6}\ K^{-1}$	$\beta = 334.6 \times 10^{-6}\ K^{-1}$
$k = 0.611\ W/m \cdot K$	$k = 0.623\ W/m \cdot K$
$\nu = 0.885 \times 10^{-6}\ m^2/s$	$\nu = 0.749 \times 10^{-6}\ m^2/s$
$Pr = 5.985$	$Pr = 5.000$

1. Frequency Uncertainty.

$$f^* = \frac{f}{\left[\frac{g\beta q''}{k}\right]^{1/2}}$$

To convert the time series to the frequency domain, a Fast Fourier Transform was performed over 1024 data points. The highest measurable frequency was determined as:

$$f_{max} = \frac{N}{2} \cdot \frac{1}{Period\ of\ Time\ Record}$$

Therfore, f_{max} = 1.97 Hz and δf=0.002 Hz. Hence,

$$\frac{\delta f^*}{f^*} = \left[\left(\frac{\delta f}{f}\right)^2 - \left(1/2\,\frac{\delta q''}{q''}\right)^2\right]^{1/2}$$

for:

$$\delta q'' = \left[\left(\frac{Q}{A^2}\delta Q\right)^2 + \left(\frac{1}{A}\delta A\right)^2\right]^{1/2}$$

and with:

Q = 27.8 W	δQ = 0.0001 W
A = 0.0081 m^2	δA = 3.6x10^{-7} m^2

then,

q" = 3432 W/m^2	δq" = 42.4 W/m^2

With,

$f = 0.425$ Hz $\qquad\qquad$ $\delta f = 0.002$ Hz

The uncertainty of $\delta f^*/f^* = 0.0078$ or 0.78%

2. Modified Grashof Number Uncertainty.

$$Gr_z^* = \left[\frac{g\beta q'' z^4}{k\nu^2}\right]$$

$$\frac{\delta Gr_z^*}{Gr_z^*} = \left[\left(\frac{\delta q''}{q''}\right)^2 + \left(4\frac{\delta L}{L}\right)^2\right]^{1/2}$$

Using the values for q" and δq" from section 1 and with z = 0.052 m and $\delta z = 0.0001$ m, then $\delta Gr_z^*/Gr_z^* = 0.0145$ or 1.45%.

3. Nusselt Number Uncertainty.

$$N_u = \frac{q'' L_c}{k(T_{plate} - T_{amb})}$$

$$\frac{\delta N_u}{N_u} = \left[\left(\frac{\delta q''}{q''}\right)^2 + \left(\frac{\delta L_c}{L_c}\right)^2 + \left(\frac{\delta \Delta T}{\Delta T}\right)^2\right]^{1/2}$$

$\Delta T = T_{plate} - T_{amb} = 17.42°C$ and $\delta\Delta T = 0.1°C$, $L_c = 0.0225$ m and $\delta L_c = 2.78 \times 10^{-4}$ m, then $\delta Nu/Nu = 0.0184$ or 1.84%

4. Rayleigh Number Uncertainty.

$$Ra = \frac{g\beta q'' L_c^4}{k\nu^2} Pr$$

$$\frac{\delta Ra}{Ra} = \left[\left(\frac{\delta q''}{q''}\right)^2 + \left(4\frac{\delta L_c}{L_c}\right)^2\right]^{1/2}$$

Then $\delta Ra/Ra = 0.051$ or 5.1%.

LIST OF REFERENCES

1. Husar, R.B., and Sparrow, E.M., "Patterns of Free Convection Flow Adjacent To Horizontal Heated Surfaces," *Int. J. Heat Mass Transfer*, v.11, pp. 1206-1208, 1968.

2. Ackroyd, J.A.D., "Laminar Natural Convection Boundary Layers on Near-Horizontal Plates," *Proc. R. Soc. London Ser. A*, v.352, pp. 249-274, 1976.

3. Goldstein, R.L., Sparrow, E.M., Jones, D.C., "Natural Convection Mass Transfer Adjacent to Horizontal Plates," *Int. J. Heat Mass Transfer*, v.16, pp. 1025-1035, 1973.

4. Lloyd, J.R., and Moran, W.R., "Natural Convection Adjacent to Horizontal Surface of Various Planforms," *J. Heat Transfer*, v.96, pp. 443-447, 1974.

5. Pera, L., and Gebhart, B., "Natural Convection Boundary Layer Flow Over Horizontal and Slightly Inclined Surfaces," *Int. J. Heat Mass Transfer*, v.16, pp. 1131-1146, 1973.

6. Pera, L., and Gebhart, B., "On the Stability of Natural Convection Boundary Layer Flow Over Horizontal and Slightly Inclined Surfaces," *Int. J. Heat Mass Transfer*, v.16, pp. 1147-1163, 1973.

7. Al-Arabi, M., and El-Riedy, M.K., "Natural Convection Heat Transfer From Isothermal Horizontal Plates of Different Shapes," *Int. J. Heat Mass Transfer*, v.19, pp. 1399-1404, 1976.

8. Hickey, C.N., "Natural Convection From a Horizontal Heater in Response to Steady and Pulsatile Input Powers," Master's Thesis, Naval Postgraduate School, Monterey, CA, June 1992.

9. Spalding, D.B., and Cruddace, R.G., "Theory of The Steady Laminar Buoyant Flow Above a Line Heat Source in a Fluid of Large Prandtl Number and Temperature-Dependent Viscosity," *Int. J. Heat Mass Transfer*, v.3, pp. 55-59, 1961.

10. Fujii, T., "Theory of the Steady Laminar Natural Convection Above a Horizontal Line Heat Source and a Point Heat Source," *Int. J. Heat Mass Transfer*, v.6, pp. 597-606, 1963.

11. Forstrom, R.J., and Sparrow, E.M., "Experiments on the Buoyant Plume Above a Heated Horizontal Wire," *Int. J. Heat Mass Transfer*, v.10, pp. 321-331, 1967.

12. Bill, R.G., and Gebhart, B., "The Transition of Plane Plumes," *Int. J. Heat Mass Transfer*, v.18., pp. 513-526, 1975.

13. Gaiser, A.O., "Natural Convection Liquid Immersion Cooling of High Density Columns of Discrete Heat Sources in a Vertical Channel," Master's Thesis, Naval Postgraduate School, Monterey, CA, June 1989.

14. Haukenes, L.O., "A Computational and Experimental Study of Flush Heat Sources in Liquids," Master's Thesis, Naval Postgraduate School, Monterey, CA, June 1990.

15. Akdeniz, E.M., "Effects of Power Pulsations on Natural Convection From Discrete Heat Sources," Master's Thesis, Naval Postgraduate School, Monterey, CA, March 1991.

16. Larsen, S., "Effects of Power Pulsations on Natural Convection From Discrete Heat Sources," Master's Thesis, Naval Postgraduate School, Monterey, CA, December 1991.

17. Incropera, F.P., and DeWitt, D.P., *Introduction to Heat Transfer*, 2d ed., John Wiley & Sons, Inc., 1985.

INITIAL DISTRIBUTION LIST

		No. Copies
1.	Defense Technical Information Center Cameron Station Alexandria VA 22304-6145	2
2.	Library, Code 052 Naval Postgraduate School Monterey CA 93943-5002	2
3.	Prof. Matthew D. Kelleher, Code ME/Kk Department of Mechanical Engineering Naval Postgraduate School Monterey, California 93943-5002	1
4.	Prof. Y. Joshi, Code Me/Ji Department of Mechanical Engineering Naval Postgraduate School Monterey, California 93943-5002	2
5.	Mr. Kip Hoffer Naval Weapons Support Center Code 6042 Crane, Indiana 47522	1
6.	Mr. Tony Buechler Naval Weapons Support Center Code 6042 Crane, Indiana 47522	1
7.	Naval Engineering Curricular Officer, Code 34 Naval Postgraduate School Monterey, California 93943-5002	1
8.	Adrian J. Jansen 2011 Whisper Wind Court Elverta, California 95626	1